SUBMILLIMETER WAVE LASERS

There are many types of submillimeter-wave lasers, including optically pumped (1), direct discharge, free-electron lasers (2), and pulsed cyclotron resonance Ge lasers (3). This article will concentrate on the most common variety, namely, optically pumped submillimeter-wave lasers. Optically pumped submillimeter-wave lasers, in turn, come in a number of versions, including continuous-wave (cw), pulse-pumped (4), and cavity-dumped (5). Within each of these categories there are a large number of variations in cavity design and pump geometry. The present article will concentrate on the most ubiquitous of these, namely, continuous-wave optically pumped submillimeter-wave lasers.

THE SUBMILLIMETER-WAVE PORTION OF THE ELECTROMAGNETIC SPECTRUM

A discussion of optically pumped submillimeter-wave lasers would not be complete without at least a brief introduction to this important region of the electromagnetic spectrum. Loosely defined, the submillimeter-wave (SMMW) portion of the spectrum, also referred to as the far-infrared (FIR), lies between the infrared and the microwave (see Fig. 1). The SMMW region, a subset of which is often referred to as the terahertz region, contains wavelengths (frequencies) from roughly 2 mm (150 GHz) to 15 μm (20 THz, 20×10^{12} Hz). This region is one of the least explored accessible areas of the electromagnetic spectrum, owing primarily to the technical difficulties that one traditionally encounters here. These difficulties are mostly associated with lack of low-loss long-distance atmospheric transmission combined with a paucity of commercially available detectors, sources, and components; although in recent times more SMMW devices have become commercially available (a trend which appears to be accelerating).

It is valuable to connect some physically intuitive concepts with the SMMW spectrum. For purposes of illustration, if one were to associate a temperature with the energy of a 1 THz photon, that would correspond to 48 K. Thus many SMMW physical effects must be observed at low temperatures so as to prevent random thermal fluctuations from disturbing the measurements.

Numerous scientifically interesting and technologically important processes take place in the SMMW region. For example, whereas molecular vibrational transitions occur in the long-wavelength infrared (IR) region, molecular rotational transitions occur in the SMMW region. Thus in order to more accurately identify molecular constituents of astronomical objects, SMMW astronomy/spectroscopy is often employed (6,7). Similarly where semiconductor valance-to-conduction band transitions typically lie in the short-wavelength infrared to long-wavelength ultraviolet (UV), hydrogenic donor and acceptor transitions (8,9) lie in the SMMW region. SMMW radiation also has the property of fairly good transmission through many plastics and composites. Thus there is interest in SMMW measurements for the characterization (10) and monitoring of plastics (11) and plastic curing processes.

HISTORICAL OVERVIEW

It would be beyond the scope of this article to provide an exhaustive discussion of any topic; therefore all discussions will be brief in nature but will provide references for the reader interested in more complete information.

Optically pumped SMMW lasers (OPSLs) were first demonstrated in 1969 and 1970 by Chang and Bridges (1). These authors produced pulsed SMMW radiation by pumping low-pressure CH_3F gas (methyl fluoride), placed in a resonator, with a Q-switched CO_2 laser. Shortly thereafter, cw SMMW lasing was produced (12). Prior to these important advances, SMMW lasers relied on discharge driven SMMW lasers (13). Producing such transitions was a very cumbersome and inefficient process requiring a combination of high current and high voltage. Additionally, these discharge-pumped SMMW lasers were comparatively limited in available lasing wavelengths. Thus, in many ways, the birth of the OPSL helped to open up the field of SMMW science and technology, by providing a readily accessible source of coherent SMMW radiation which covered the entire SMMW spectrum (in the form of discrete, limited-tunability, laser lines). Note that tuning can be added to OPSL output via sideband generation (14–16). Numerous review articles on OPSLs have been published through the years (17–19), any of which is a good source for more OPSL information.

OPERATIONAL OVERVIEW

A generalized schematic representation of an OPSL system is presented in Fig. 2. The SMMW laser cell consists of the following: a vacuum envelope in which a molecular gas at low pressure is placed, some source of optical feedback (end mirrors), and a method of admitting IR pump radiation and emitting SMMW radiation. A grating-tuned CO_2 laser (emission in the 9 μm to 11 μm range) is typically used to pump the SMMW laser. This pump radiation is often admitted into the OPSL cavity through a small input-coupling hole in one end mirror. The SMMW radiation produced in the OPSL is then typically emitted through either an output-coupling hole or

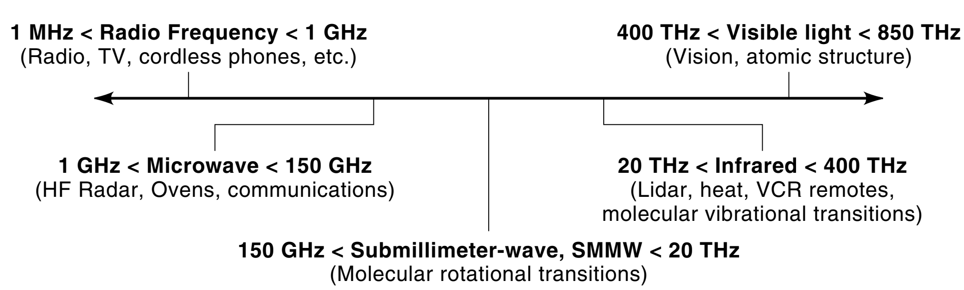

Figure 1. Subset of the electromagnetic spectrum, SMMW region highlighted.

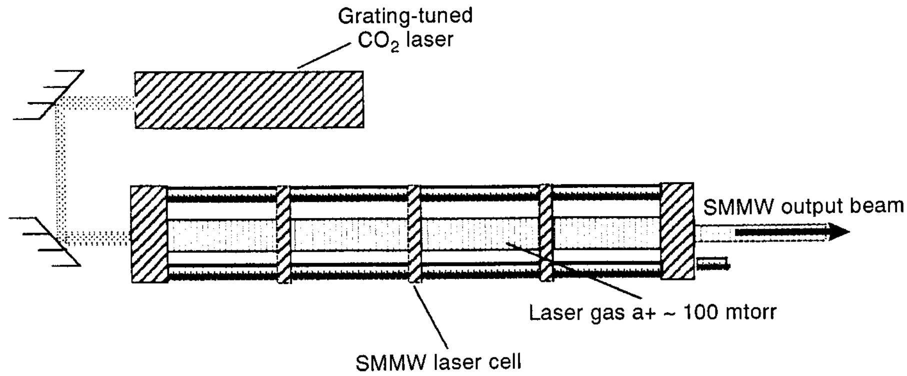

Figure 2. Schematic diagram of a general OPSL system.

some sort of uniform output coupler (20). To understand how this device produces SMMW radiation, one must examine the quantum-mechanical molecular processes which take place. The present section will provide only a very general overview of these processes; a more thorough discussion will follow in the section entitled "Continuous-Wave Optically Pumped Submillimeter-Wave Lasers: In Detail."

OPSLs all operate on molecular rotational transitions. For purposes of illustration we will consider a specific OPSL example for explanation. A representative diagram of the operation of an OPSL, operating on the 118.83 μm line in methanol, is presented in Fig. 3(a), an illustration of the origin of the methanol quantum numbers is presented in Fig. 3(b), and a physical diagram of the lasing process is presented in Fig. 4. In the lasing process: (1) an IR photon with an energy which *very* closely matches a transition from a particular rotational state in the ground vibrational manifold to a rotational state in an excited vibrational manifold is absorbed by a gas molecule; (2) if the conditions are correct, this process causes a population inversion between rotational states; (3) the inverted rotational transition lases and emits in the SMMW, either in the excited manifold due to the pumping, or in the lower manifold due to depletion of the lower state; and (4) the molecule is left in the excited vibrational manifold and must return to the ground manifold before it can participate in a cw lasing process again.

A physical diagram of the lasing process of Fig. 3 is provided for further illustration in Fig. 4. In this example the 9.69 μm IR photon excites the C–O stretch mode. The molecule then lases between the $J = 16$ and $J = 15$ rotational levels, emitting a photon at 118.83 μm.

With the large energy difference between the rotational and vibrational energy level separations, one might expect the lasing process to be quite inefficient. This is in fact the case. The majority of the pump radiation is simply converted to heat. The theoretical limit on efficiency for the OPSL is given by the well-known Manley–Rowe limit (21):

$$\epsilon = \frac{\nu_{\mathrm{FIR}}}{2\,\nu_{\mathrm{IR}}} \tag{1}$$

where ϵ is the efficiency of converting pump radiation into SMMW radiation, ν_{FIR} is the frequency of the emitted SMMW photons, and ν_{IR} is the frequency of the pump photons. So for example, for the 118.83 μm laser line in CH_3OH the efficiency limit is 4%. Typical efficiency at this transition is on the order of 0.2%, and the best reported efficiency (22) is 1% for high power operation and is 0.8% for high-efficiency lower power operation (37). This example is one of the higher efficiency transitions; typical OPSL efficiencies are in the range of 0.005% to 0.1%.

TYPICAL PERFORMANCE AND APPLICATIONS

OPSL lines are available throughout the SMMW spectrum. Some of the stronger examples and their published output powers are indicated in Fig. 5. In general, once one has an OPSL system, virtually any of the available lines can be obtained by a combination of (1) introduction of the appropriate gas into the SMMW resonator, (2) operation of the pump laser at the corresponding line, and (3) tuning of the SMMW cavity

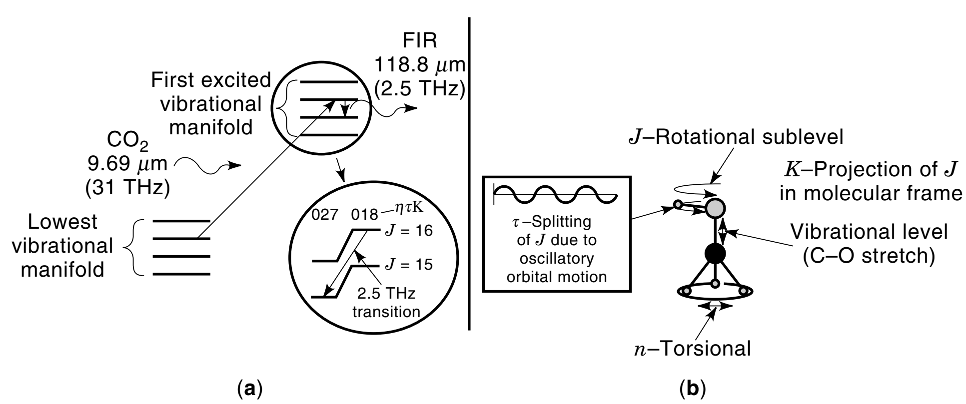

Figure 3. (a) Schematic energy diagram of 2.5 THz methanol laser. (b) Illustration of methanol quantum numbers; the top "large" atom is oxygen, the bottom "large" atom is carbon, and the rest are hydrogen.

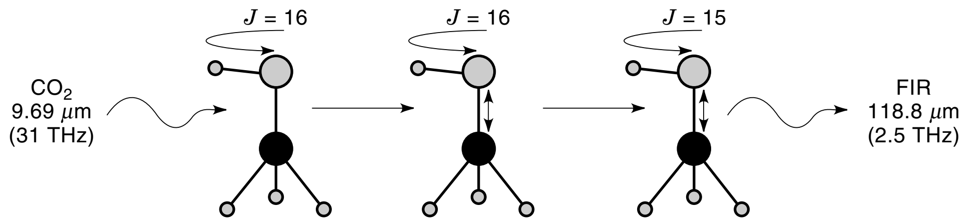

Figure 4. Physical representation of the 2.5 THz lasing process in methanol.

to the correct length. Thus OPSLs offer great versatility after the initial capital investment.

It should be noted that in the past, both the pump laser and the SMMW laser have typically been of either the flowing gas or short-term sealed-off types. As a result, the maintenance and consumable costs have been considerable. However, in the recent past the same all-metal-seals, ultra-high-vacuum technology which has led to no-service CO_2 industrial and scientific lasers (24), has begun to be applied to OPSLs. These advancements are expected to dramatically improve the service interval of OPSLs.

For those interested in operating an OPSL system, a fairly thorough listing of OPSL lines is available from CRC Press (25) and other sources (26,26a) and more lines are discovered and published every year (27). It should be remembered that the output powers shown in Fig. 5 represent published results; more output power can often be obtained either by SMMW resonator optimization for a given line or by pumping with a higher-power pump laser. The data at 1.6 and 2.5 THz already represent high-efficiency results obtained with optimized, high-pump power, laser systems.

Along with the versatility offered by OPSLs comes a certain degree of complexity. While it is possible to construct a functional OPSL fairly easily, design and construction of a robust, reliable OPSL requires a fair degree of sophistication on the part of the system architect. Many experimentalists have experienced frustration in trying to obtain data with unreliable, poorly engineered OPSLs. The resulting anecdotes have plagued the OPSL business. However, in recent years it is becoming increasingly clear that properly engineered OPSLs can offer high reliability and round-the-clock unsupervised operation for months or more. As an example, the 2.5 THz local oscillator for NASA's CHEM 1 satellite is an OPSL under construction by DeMaria ElectroOptics Systems (23). This OPSL will operate autonomously in space on a 5 year atmospheric measurement mission. Another example is the fully autonomous, wavelength-tunable, SIFIR laser under development at DEOS for Goddard Space Flight Center (47).

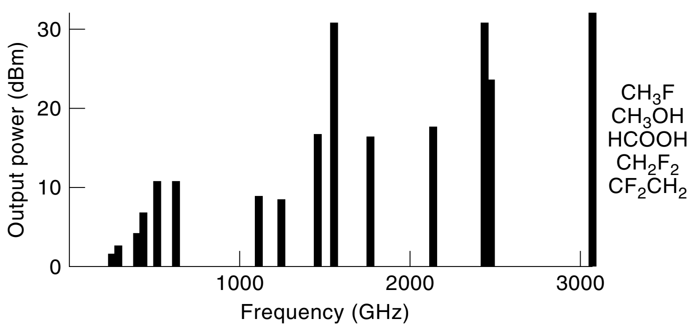

Figure 5. Histogram of some of the stronger OPSL lines.

The applications of OPSLs are just beginning to take shape. As the reliability of the OPSL becomes more established, it is expected that its applications will grow as well. Some of the typical applications in place today are: semiconductor spectroscopy, radar scale modeling (28), plasma diagnostics (29), and local oscillator sources for heterodyne radiometry (23). OPSLs have also found application in plastics/polymer inspection (11), an area which is expected to grow in the future.

CONTINUOUS-WAVE OPTICALLY PUMPED SUBMILLIMETER-WAVE LASERS: IN DETAIL

Theory of Operation

This section is intended to provide a more in-depth coverage of the theory of operation of OPSLs and is organized into subsections as follows: "Cavity Configurations," "OPSL Modeling," "Frequency Stability and Laser Tune-Up," and "Amplitude Stability." The first subsection is intended to provide a physical picture of some of the typical OPSL cavity arrangements. The second subsection provides a mathematical framework for understanding OPSLs, and the remaining two subsections give some detailed information concerning the operation and stability of OPSLs.

Cavity Configurations. A large variety of cavity configurations have been devised for OPSLs. Some of the more typical examples are presented in Fig. 6. It should be noted that standing-wave, axially pumped OPSLs are the most common variety and thus will be referred to in this article as "typical." Furthermore, more attention will be given to standing-wave OPSL issues in this article than to issues specific to other OPSL configurations.

Both the zigzag and transversely pumped versions [Fig. 6(d,e)] offer some degree of decoupling of the pump and emission frequency (see section entitled "Frequency Stability and Laser Tune-up"), but unfortunately also provide significantly less than optimal efficiency. The ring version (f) offers less susceptibility to SMMW feedback, immunity to pump feedback, and immunity to "two-photon-light-shift" effects (30). Unfortunately the ring configuration also provides less than optimal efficiency (30), output direction switching, and significant complications for optimal output coupling. The Gaussian resonator [Fig. 6(b)] is very useful when a small internal beam size is desired, such as in a cavity-dumped laser (5). The half-symmetric Gaussian resonator [Fig. 6(a)] and the waveguide resonator [Fig. 6(c)] are probably the most common configurations in use. The half-symmetric Gaussian, combined with a standard hole output coupler, is an excellent choice where optimal efficiency and mode purity take a back seat to easy change of output line (e.g., spectroscopy applica-

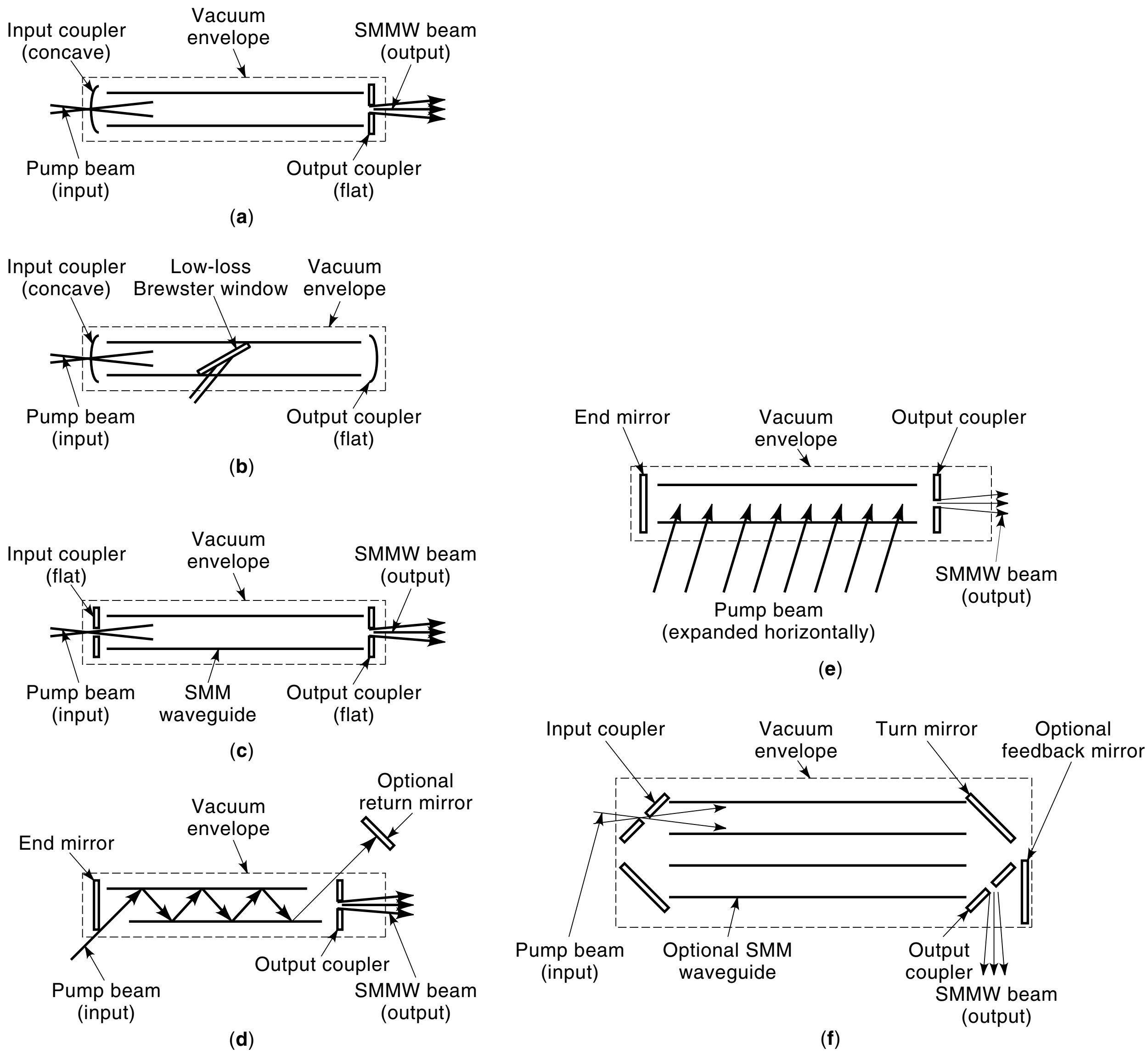

Figure 6. Typical OPSL cavity configurations. (a) Half-symmetric Gaussian resonator. (b) Gaussian resonator. (c) Waveguide resonator. (d) “Zigzag” pumped resonator. (e) Transversely pumped resonator. (f) Ring resonator.

tions and detector development). The dielectric waveguide resonator is an excellent choice when efficiency and mode purity are paramount. While a metal, overmoded waveguide can be used with this resonator configuration, such a laser will typically emit a large number of transverse modes simultaneously (31), with the specific spectrum changing erratically over time.

With any cavity, output coupling is an important issue. The transverse and zigzag pumped configurations separate the pump and SMMW radiation, thereby allowing the output coupler to only need specific optical properties in the SMMW region. All of the other cavity configurations described require that the output coupler have specific optical properties at both the pump and SMMW frequency simultaneously. Ideally the output coupler would have 100% reflection at the pump frequency and some predetermined (<100%) reflectivity at the SMMW frequency (typically in the range of 85% to 95%).

The simplest form for the output coupler is the well-known hole coupler. In this embodiment the output coupler is a “100 %” mirror with a central hole. Typical hole diameters are on the order of 4 mm to 5 mm, depending on the effective mirror outer diameter and the gain of the SMMW line. Since such an output coupler does not provide a vacuum window, one must be employed following the output coupler. This window must pass the SMMW radiation, and it might be desirable that it reflect or absorb any pump radiation which propagates through the output coupling hole.

Where higher efficiency and mode purity are required, a uniform output coupler is desired. This device is dichroic in nature. The dichroism can be accomplished in a number of ways. Some of the more typical versions are arrays or grids of small metal structures fabricated on a coated substrate (32). These form a frequency-selective surface. The substrate is made of a material which has low absorption in the SMMW

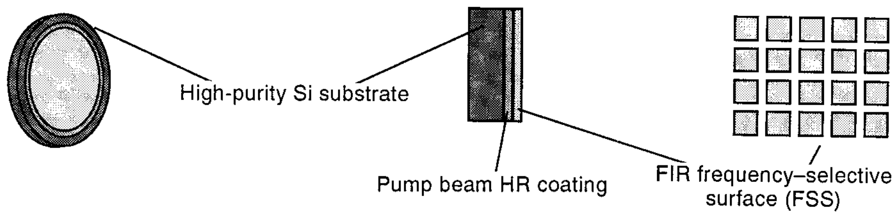

Figure 7. Representative diagram of a uniform output coupler for an OPSL.

and may then be coated with a dielectric high-reflectivity coating for the pump frequency. Great care must be taken to insure the lowest SMMW loss for the high-reflectivity coating, lest a great deal of the SMMW output will be lost to this absorption. A representative diagram of a uniform output coupler is presented in Fig. 7.

OPSL Modeling. Modeling of OPSLs has received a great deal of attention through the years. While the physical/rate equation models are extremely useful in elucidating key parameters and influences on OPSL performance, they do not in general provide the most accurate predictive results. However, phenomenological modeling, combined with careful attention to the physical and rate equation results, can yield excellent predictive and scaling results.

Physical/Rate Equation Models. A number of excellent rate equation model results for OPSLs have been published over the years (33–35). While these works have produced a number of important results, only a very small subset will be covered here.

Theoretical Framework. An energy-level model of a typical OPSL (similar to the diagram of Fig. 3) is represented in Fig. 8 (34). This is a typical four-level system where the levels are as follows: 0, lower rotational sublevel of the pump transition in the ground vibrational manifold; 1, lower laser level (rotational sublevel) in the excited vibrational manifold; 2, upper laser level (rotational sublevel) in the excited vibrational manifold (assumed here to be the upper pump transition level); and 3, ensemble of all of the other rotational sublevels in the excited vibrational manifold. In some OPSLs there is a cascade process which populates the upper laser level after the pump has populated a level above the upper laser level.

The rate of pump excitation is w_p, the rate of equilibration of rotational levels within a vibrational level is w_r and is on the order of 10^7/s to 10^8/s [these levels are collision (pressure) broadened], and the rate of deexcitation back down to the lower vibrational manifold is w_v and is on the order of 10^5/s to 10^6/s (36) [these levels are velocity (Doppler) broadened at typical operating pressures]. The reason for the mixed broadening is that the cross section for change of rotational state upon collision is orders of magnitude larger than that for change of vibrational state, $w_r \gg w_v$.

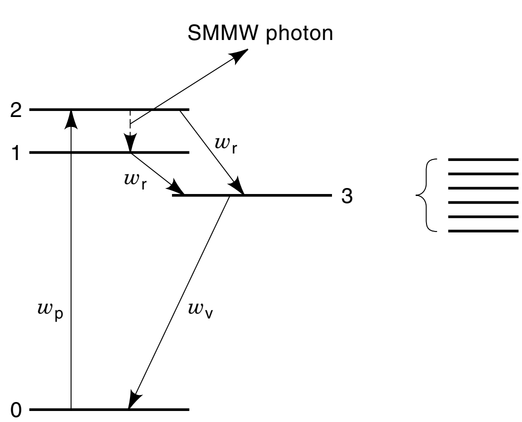

Figure 8. Energy-level model for an OPSL.

It should now be clear that the pumping mechanism must be extremely specific if a population inversion is to be maintained. If a pump source having a spectrum encompassing several rotational sublevels were used, then the rotational relaxation rate would be expected to prevent any population inversion buildup. This situation differs substantially with many other laser systems, where the pump merely has to populate above the upper laser level which will then be naturally filled by the inherent transition probability differences. In these systems the pump can be very broad indeed, often using flashlamps or electrical discharge for excitation. Of course, in some systems, discharge pumping can be somewhat specific. The CO_2 laser is a good example, where the discharge-pumped N_2 level is chosen to closely match the desired excitation level of CO_2.

The presence of the other rotational sublevels in the excited vibrational manifold not only provides a path to unwanted loss of population in the upper laser level, but also helps to empty the lower level (helping to maintain inversion). If collisions are equally likely to depopulate both levels 1 and 2, but the pump source is preferentially populating level 2, then level 1 will tend to have a lower population than level 2 (population inversion), and the molecules in 2 will have many equally likely levels to go to via collisions; thus the nonradiative $2 \rightarrow 1$ transition should not significantly degrade the inversion. If the other rotational sublevels were not present, then after emission of an SMMW photon the lower level would have to depopulate via a vibrational transition. This rate is so slow that the population inversion would be significantly degraded in cw operations, and the lasing might be expected to cease. In pulsed OPSLs the constraints are less severe in that the lasing process can take place before many of the nonradiative deexcitation mechanisms can take effect. Thus in pulsed operation, many more lines are accessible and the lines typically operate at higher pressure.

This seems an appropriate place to discuss a topic related to vibrational transition broadening, namely, vibrational bottle-necking. A fairly recent measurement of the order of magnitude of the vibrational bottle-neck time has provided data important to understanding the processes which control the efficiency of OPSLs (36). In that work the authors were able to demonstrate, at pressures similar to that typical of cw OPSLs, a linear relation of FIR average power with pump-pulse repetition rate up to at least 100 kHz, suggesting a vibrational relaxation rate of at least 10^5 s^{-1}. Since the vibrational relaxation processes in the laser are complex, involving energy exchange not only with other gas molecules but also directly with the laser tube walls, a direct calculation of the relaxation rate appears intractable. Thus the experiment of Ref. 36 provided the first direct, in laser, measure of the timescale of the bottle-necking effect.

Setting up the rate equations commensurate with Fig. 8, a number of important results can be obtained (34). In particular, the output power versus input power and pressure may be obtained. With suitable approximations (any of: $p \ll p_s$, $U \ll U_s U \gg U_s$), the general form is given by

$$P_{\mathrm{FIR}} = tQ\frac{\nu_{\mathrm{FIR}}}{\nu_{\mathrm{IR}}}\left[\frac{1}{t+a}\frac{p/p_s}{1+p/p_s}\frac{U}{1+U/U_s} - \frac{p^2}{G}\right] \tag{2}$$

where

$$G = \frac{Lc^2\xi}{2\pi^3\nu_{\mathrm{FIR}}^2 t_{\mathrm{sp}} C^2 V h\nu_{\mathrm{IR}}} f(\nu) \quad \text{and} \quad Q = \xi\frac{g_1}{g_1+g_2}$$

where t is the FIR coupling loss, a is the FIR loss to other sources, L is the active laser length, p is the internal pressure, U is the input pump power (in suitable units), $f(\nu)$ is the normalized Lorentzian of width $\Delta\nu_N$ ($\Delta\nu_N = w_r/\pi = Cp$), ν_{FIR} and ν_{IR} are the respective FIR and pump radiation frequencies, t_{sp} is the spontaneous lifetime of level 2, C is the constant which relates w_r to pressure, ξ is the fraction of the pump power which pumps the $0 \rightarrow 2$ transition, p_s is the pressure where the pump absorbed in the gas equals the pump lost to all other sources (i.e., wall losses, etc.), U_s is directly related to the saturation power of the pump transition, and g_i denotes the degeneracy of state i.

Examining Eq. (2), FIR output will increase linearly with U for $U \ll U_s$ and will then saturate for $U \gg U_s$. The FIR output will begin proportional to p, maximize, and then decrease to zero at some high pressure. If a series of further approximations are made, then an interesting conclusion related to the optimal operating pressure, p_{opt}, is reached, namely:

$$p_{\mathrm{opt}}\ \alpha\ U \qquad \text{for } p \ll p_s$$

and

$$p_{\mathrm{opt}}\ \alpha\ U^{1/3} \qquad \text{for } p \gg p$$

At low pump powers, very good agreement with the above relations has been obtained for the strong line at 118.83 μm in CH_3OH.

An example of the tuning of the OPSL output power with pressure and pump power is presented in Fig. 9 (37). As shown there, as the input power is increased, the optimal pressure increases. Further evaluation of these data has shown good agreement with the general pressure relations presented above.

Physical Theory. While the above discussion has provided a theoretical framework for OPSLs, a theory which only contacts direct variables is also desired. As an example of a "first-principles" physical theory for the 118.83 μm OPSL in CH_3OH, consider the following self-consistent model (35). This model is introduced here merely to provide the reader with exposure to the general form of the equations that govern OPSL operation. Reference 35 should be consulted if more in-depth knowledge is desired. It must be remembered that this model still requires either some experimentally determined input or significant approximations for predictions and is therefore self-consistent instead of purely predictive. However, the model does provide insight into the physical parameters and processes in OPSLs. Following a rate equation approach, one arrives at an expression for the gain at the center of the FIR transition:

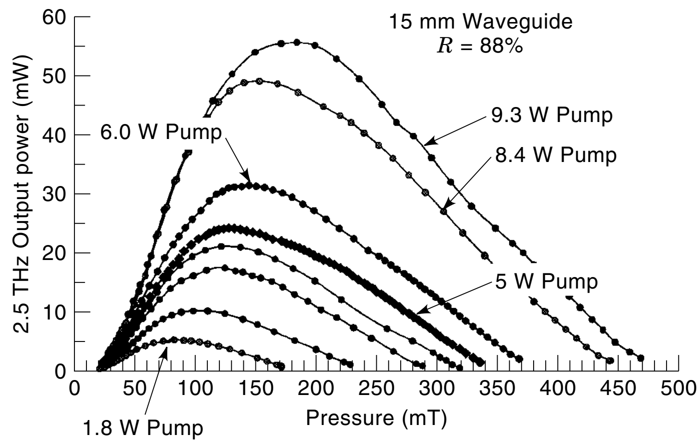

Figure 9. OPSL output power versus pump power and operating pressure.

$$g_{\mathrm{FIR}} = \int_{-\infty}^{\infty}\left(\frac{h\nu_{\mathrm{FIR}}L_0(v,\nu_{\mathrm{FIR}})}{\left(1+\dfrac{g_2}{g_1}\right)I_{\mathrm{SAT}}}\right)\left\{\frac{S(v)-\gamma_r\left(\dfrac{g_2}{g_1}f_1-f_2\right)\left(\dfrac{1}{\Gamma_v}\displaystyle\int_{-\infty}^{\infty}S(v)\,dv+f_M^e N_0\right)f(v)}{\left(1+2\dfrac{I_{\mathrm{FIR}}}{I_{\mathrm{SAT}}}L_0(v,\nu_{\mathrm{FIR}})\right)}\right\}dv \tag{3}$$

The first term in the bracket in Eq. (3) represents the FIR gain contribution from active molecules (35), while the second term is related to excited-state FIR absorption (38). The following terms are defined (35):

- g_2 and g_1 are the degeneracy degrees of upper and lower FIR lasing levels, respectively (39):

$$\frac{g_2}{g_1} = 1.065$$

- f_2 and f_1 are the population equilibrium fractions of these levels within the upper vibrational manifold (40):

$$f_2 = 1.83\times10^{-3}, \qquad f_1 = 2.64\times10^{-3}$$

- f_M^e is the equilibrium fraction of the upper vibrational state referred to the total number of molecules per unit volume (40):

$$f_M^e = 6.78\times10^{-3}$$

- N_o is the total number of molecules per unit volume.

- I_{SAT} is the FIR saturation intensity:

Ref. 35 gives 2.5 W cm^{-2} torr^{-2}

- $L_0(v,\ \nu_{FIR})$ is the normalized Lorentzian function of full width $= \lambda_{FIR}\Delta\nu_H$ which enters into the FIR emission cross section, where $\Delta\nu_H$ is the homogeneous linewidth (35):

$$\Delta\nu_H = 28\,\text{MHz torr}^{-1}$$

- $\gamma_r = \pi\Delta\nu_H$ is the rotational relaxation rate.
- Γ_v is the vibrational relaxation rate, related to w_v in the last section.
- $S(v) = S^+(v) + S^-(v)$ is the pump source term, where $S^{\pm}(v)\,dv$ represents the number of molecules in the velocity range v to $v + dv$ which are pumped per unit volume per unit time by the forward and backward circulating CO_2 IR pump beam:

$$S^{\pm}(\nu)\,d\nu = \frac{I_{IR}^{\pm}}{h\nu_{IR}}\frac{\lambda_{IR}\Delta\nu_H}{\pi}\frac{\alpha_0 e^{-v^2/\Delta v^2}}{v^2 + \dfrac{\lambda_{IR}\Delta\nu_H}{2}\sqrt{1+\dfrac{I_{IR}^{+}+I_{IR}^{-}}{I_0}}}$$

- $f(v)$ is the Maxwellian velocity distribution of width $2\Delta v = 2\sqrt{2k_BT/m}$ and is related to the Doppler widths of the pump and lasing transitions.

Before attempting to integrate Eq. (3) and utilize the result to predict the FIR output power, a number of simplifications are made. First, treating the IR intensity as if it is constant for both directions and radially uniform (this approximation is not particularly accurate) (41) and assuming that the IR absorption coefficient, FIR intensity, and FIR gain are similarly uniform, we can define a pump intensity I_{IR} (33) given by

$$I_{IR} = \frac{P_{IR}}{2A}\left(\frac{1}{\alpha L + \beta_{IR}}\right) \tag{4}$$

where P_{IR} is the input pump power in watts, A is the FIR guide area in cm^2, L is the cavity length in cm, β_{IR} is the IR per-pass loss to mechanisms other than the FIR gas, and α is the saturated IR absorption coefficient given by

$$\alpha = \frac{\alpha_0}{\sqrt{1+\dfrac{I_{IR}}{I_s}}} \tag{5}$$

where I_s is the IR transition saturation intensity (Ref. 35 gives I_s = 169 W cm^{-2} torr^{-2}).

With these approximations [and rate equation results for the pump transition (35)], and noting that the FIR output power $P_{FIR} = 2tAI_{FIR}$ (where t is the output coupling fraction), we may find an analytic expression for the FIR output power:

$$P_{FIR} = tAI_{SAT}\left\{\frac{I_{IR}}{t}\eta F_{abs}F_{trans}\frac{1}{I_{SAT}} - 1\right\} \tag{6}$$

where

$$\eta = \left[\frac{1}{1+\dfrac{g_2}{g_1}}\right]\frac{\nu_{FIR}}{\nu_{IR}} \tag{7}$$

is the quantum efficiency,

$$F_{abs} = \frac{\alpha L}{\alpha L + \beta_{IR}} \tag{8}$$

is the fraction of pump power absorbed in the gas, and

$$F_{trans} = \left[\frac{t(1-A_e)}{t+a}\right]\frac{1}{1+h} \tag{9}$$

is the fractional transmission loss of the FIR radiation, where

$$A_e = \gamma_r\left(\frac{g_2}{g_1}f_1 - f_2\right)\left(\frac{1}{\Gamma_v} + N_0 f_M^e \frac{h\nu_{IR}}{2I_{IR}\alpha}\right)\rho(\delta v/\Delta v)$$

and is related to FIR excited state absorption,

$$\rho(\delta v/\Delta v) = \int_{-\infty}^{\infty} f(v)L(v,\nu_{FIR})\,dv$$

and

$$h = \frac{\lambda_{IR}}{\lambda_{FIR}}\frac{\sqrt{1+2\dfrac{I_{IR}}{I_s}}}{\sqrt{1+2\dfrac{I_{FIR}}{I_{SAT}}}}$$

and is related to hole burning.

To develop an intuitive feeling for the order of magnitude of some of the quantities here, consider the following two graphs. In Fig. 10, the saturation degree of the pump transition for the 118.8 μm line is presented. As shown there, over this range of pump power this laser's pump transition will be in the moderate saturation regime; thus neither the strong or weak saturation simplifications are applicable. Many other OPSL lines operate in the same regime.

Another quantity of interest is the fraction of pump power absorbed by the laser gas. Using the same example as above, this result is presented in Fig. 11. As shown there, the fractional absorption increases rapidly as a function of β. Therefore it is expected that the efficiency of the OPSL will be a strong function of β.

Phenomenological Modeling. While the physical theory outlined in the section entitled "Physical/Rate Equation Models" provides a good starting point, it is desirable to have a simple predictive theory of the laser's performance wherein design parameters can be adjusted and then the laser's output predicted. To that end, a phenomenological theory of the laser's operation in terms of observed "lumped-sum" quantities, such as gain and saturation intensity, has been developed. These quantities may be determined by fitting a distributed-loss Rigrod model (42) to the output power data obtained as a function of output coupling percentage. From Eqs. (16) and (19) in

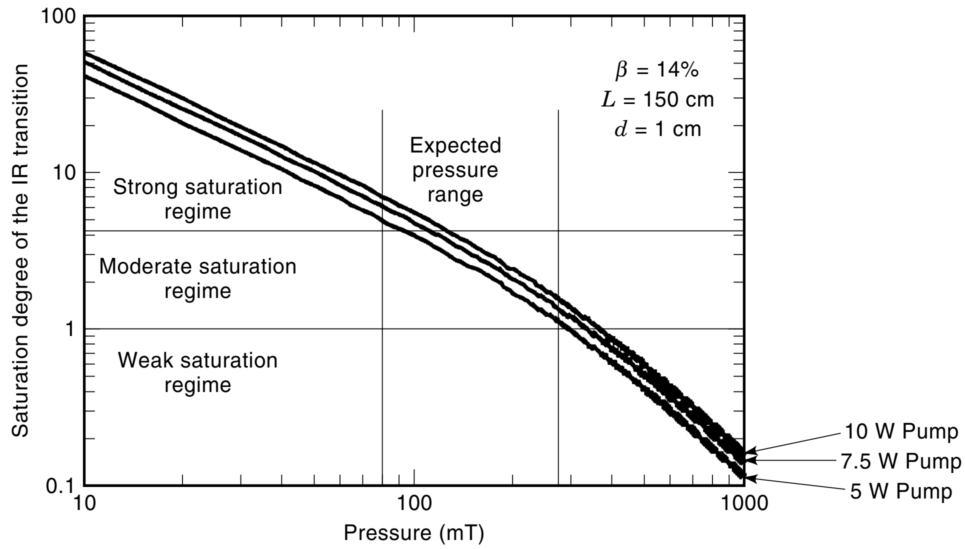

Figure 10. Saturation degree of the vibrational pump transition for the 118.8 μm laser line in CH_3OH. This figure is calculated for a laser having a guide diameter of 10 mm, and a length of 150 cm and assuming a β of 14%. The three curves are for different pump laser input power levels.

Ref. 42, one can derive

$$P_{\mathrm{FIR}} = P_{\mathrm{SAT}}(1 - l_{\mathrm{mc}} - r_2) \left\{ \frac{[L(\gamma_0 - \alpha_0) + \ln\sqrt{r_1 r_2}\,]}{\left(1 + \sqrt{\frac{r_2}{r_1}} - \sqrt{r_1 r_2} - r_2\right)\left[1 - \frac{\alpha_0 L}{\ln\sqrt{r_1 r_2}}\right]} \right\} \tag{10}$$

where L is the active cavity length in cm, γ_0 is the small-signal gain in cm^{-1}, α_0 is the guide loss in cm^{-1}, r_2 is the reflectivity of the output coupler, l_{mc} is the guide-mirror coupling loss, and

$$r_1 = 1 - \mathrm{IC}_{\text{hole loss}} - l_{\mathrm{mc}} (\mathrm{IC}_{\text{hole loss}} \text{ is the loss introduced by the input coupling hole})$$

Equation (10) can be fit to output power versus output coupling and the relevant Rigrod parameters can thereby be determined. These results permit later prediction of laser performance as a function of cavity parameters and provide information vital to understanding the operating regime of the laser. An example of such a fitting procedure for two different cavity configurations, both operating on the 118.83 μm laser line and at the same pump power (5 W), is presented in Fig. 12. The values for the Rigrod parameters for these fits are in the respective ranges $P_{\mathrm{SAT}} \sim 320$ mW to 190 mW, total internal loss ~1% to 7%, and small signal gain ~0.12% to 0.24%/cm.

Examination of Eq. (10), in different gain/loss regimes, illustrates critical design issues. For example, the OPSL system being employed in the NASA CHEM 1 satellite operates in the low-gain, low-loss regime (23). Therefore very small changes in loss can have considerable effects on overall performance. More detail on this example is found in the section entitled "An Example OPSL System: The NASA CHEM 1 Satellite, 2.5 THz Laser Local Oscillator." In the high-gain high-loss regime, small changes in loss do not have a substantial effect on output power. Very few, if any, cw OPSLs operate in the high-gain high-loss regime.

Frequency Stability and Laser Tune-up. A properly designed OPSL can provide a high degree of frequency stability and

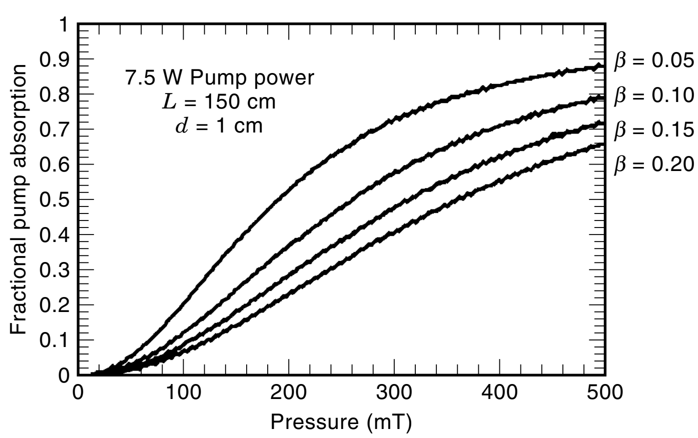

Figure 11. Fractional pump power absorption versus pressure. The four curves are for different values of β. The laser parameters assumed are the same as for Fig. 10, but the pump power is held fixed at 7.5 W.

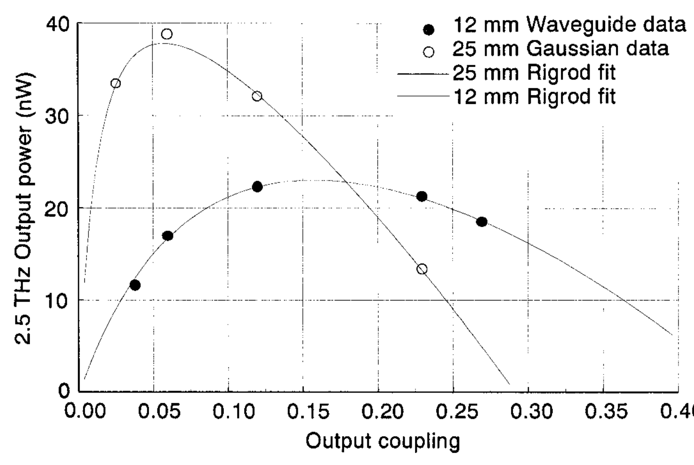

Figure 12. Output power versus output coupling, for three different cavity configurations.

repeatability. The repeatability can be significantly effected by cavity design, tune-up procedure, and pump frequency locking technique. If a standing-wave OPSL is used, as is most common, there can also be a pressure dependence (43). The repeatability will be a function of the design, tune-up, and frequency control procedure. While the natural linewidth of a typical OPSL may be on the order of millihertz, a number of factors typically degrade this significantly.

While from the simple relation (44)

$$\Delta\nu = \left\{ \frac{[2\pi h\nu_0(\Delta\nu_{1/2})^2\mu]}{P} \right\} \tag{11}$$

where $\Delta\nu$ is the linewidth, $\Delta\nu_{1/2}$ is the full width of the passive cavity resonance, h is Planck's constant, ν_0 is the center frequency of the laser transition, μ is the population inversion factor (1 in an ideal four-level laser), and P is the output power of the laser, the short-term linewidth of an OPSL might be expected to be on the order of $<$1 mHz, there are a number of processes which degrade the frequency stability of OPSLs. The simplest of these are cavity length fluctuations induced by mechanically coupled mirror vibrations. The magnitude of this effect can be easily estimated with

$$\Delta\nu_{\text{vib}} \approx \nu \left\{ \frac{\Delta L}{L} \right\} \tag{12}$$

where L is the OPSL nominal cavity length, ΔL is the mechanically coupled change in cavity length, ν is the nominal OPSL operating frequency, and $\Delta\nu_{\text{vib}}$ is the resulting frequency change. The reader may note that this approximation is merely a nonactive cavity calculation and also assumes that the cavity is many wavelengths long. Also, gain-induced frequency pulling will reduce the Eq. (12) result slightly. To give the reader a feel for typically achieved results, note that the best nonvibrationally stabilized OPSLs operating at 2 THz have vibrationally induced linewidths of ~30 kHz (this corresponds to ~20 nm of mirror motion), and more typical results are on the order of 150 kHz (this corresponds to ~100 nm of mirror motion). Even better results can be achieved if active vibrational stabilization is employed, providing that the pump source is of sufficient spectral purity.

As described in the section entitled "Operational Overview," all OPSLs operate on molecular rotational transitions. However, it may not be immediately obvious that the pump (vibrational) transition is Doppler-broadened, while the lasing (rotational) transition is pressure-broadened. Thus the typical OPSL process is mixed-broadened. This complication has many impacts on frequency stability and therefore on design considerations.

As described in the section entitled "Physical/Rate Equation Models," the reason for the mixed broadening is that the cross section for changing of vibrational state upon collision with another gas molecule is orders of magnitude smaller than that for changing of rotational state. Thus the rotational levels are homogenized on a time scale of tens of nanoseconds, whereas the vibrational levels are not homogenized at the typical operating pressures. These conditions lead to a situation where the vibrational transition is inhomogeneously Doppler-broadened while the rotational transitions are homogeneously pressure-broadened.

The mixed broadened nature of the OPSL, combined with other properties, lead to a number of important design considerations. In a typical OPSL, an excited molecule will lase prior to undergoing an inelastic, velocity-changing collision (45). This effect is often called "velocity memory." The Doppler width of the vibrational transition will be on the order of 50 MHz, and the integrated width of a well-behaved pump laser will be on the order of 50 kHz. Thus the pump radiation directly interacts with only a limited portion of the Doppler line (45a). The velocity memory effect, combined with the limited pump field interaction with the vibrational line, serves to couple the OPSL frequency stability with the pump laser frequency stability. The Doppler portion of this coupling can be expressed as

$$\text{FM}_{\text{FIR}} = \text{FM}_{\text{pump}} \left\{ \frac{\nu_{\text{FIR}}}{\nu_{\text{pump}}} \right\} \tag{13}$$

where FM_{FIR} is the Doppler-coupling-induced FIR frequency modulation, FM_{pump} is the FM dither impressed on the pump laser, ν_{FIR} is the FIR operating frequency, and ν_{pump} is the pump frequency.

With this information in mind, it becomes clear that the tuning of an OPSL system can tend to be an iterative process, unless one has a priori independent knowledge of the precise pump frequency (independent pump frequency knowledge is not typical of OPSL systems, but several such OPSL systems have been operated) (46,47). The operator of the system will typically adjust the cavity length of the OPSL until emission is observed. Over the majority of the cavity length, no SMMW emission will be observed because the typical OPSL operable linewidths are on the order of 10 MHz. The operator then adjusts the pump frequency within its tuning range to optimize OPSL output power, then returns to the OPSL cavity length adjustment, and so on. This process effectively "walks" both lasers toward the optimal OPSL efficiency point in frequency. For a standing-wave OPSL, the maximum efficiency is achieved when pumping off vibrational line-center. This is due to the fact that the optimal efficiency is a function of the total number of molecules available to participate in the lasing process. While the Doppler-broadened line's absorption coefficient peaks at line center, since the pump field will be propagating in both directions, two velocity groups may be excited by pumping off line-center; thus the total number of excited molecules when pumping off line center will exceed the total number when pumping on line center, even though the absorption on line center is greater. The frequency of operation resulting from iterative tuning may or may not correspond to OPSL transition line center, depending on the cavity design and on a number of interacting efficiency and feedback effects.

In effect the selection of OPSL cavity length selects the velocity groups which best contribute to the lasing process. It is this feature which makes the absolute frequency of a typical OPSL vary from tune-up to tune-up (on the order of 2 MHz), depending on the care taken by the operator. This effect can be avoided in a system with an independent absolute pump frequency lock. In such a system the pumped velocity group can be independently selected and then the OPSL output optimized. The resulting OPSL absolute frequency can be extremely reproducible if great care is taken in OPSL cavity tune-up and pressure repeatability, or if a transversely pumped cavity is employed (43) and if the absolute two-photon regime is avoided when working with a standing-wave cavity (46).

The above discussion does not exhaust the OPSL frequency stability issues. In standing-wave OPSLs, another curious frequency stability effect has been observed, namely, the two-photon light shift (TPLS). The TPLS can be thought of as a high-frequency Stark effect induced by interaction of the Doppler-broadened vibrational transition with the pump field. This is a manifestly coherent effect, related directly to the coherent pump employed (in contrast to, say, discharge pumping of other types of gas lasers). This effect is directly related to Autler–Townes splitting (48).

The general form of the TPLS effect is given by (49)

$$\Delta\nu_{\mathrm{FIR}} = \frac{\left[-\Delta_{\mathrm{f}} - \dfrac{\beta^2 \cdot \Delta_{\mathrm{p}}}{2 \cdot \Delta_{\mathrm{p}}^2 + \dfrac{\gamma^2}{8}}\right]}{1 + 2 \cdot \pi \cdot \dfrac{\gamma}{\mathrm{c} \cdot \alpha}} \tag{14}$$

where Δ_f is the FIR cavity offset from FIR line center, γ is the vibrational and rotational (assumed same) homogeneous linewidth, Δ_p is the pump laser frequency offset from the vibrational transition line center, β is the Rabi frequency for the pump transition, α is the FIR gain per unit length, and the factor in the denominator is the FIR gain-reduced pulling factor. It should be noted that β is in general, proportional to the pump field magnitude (which is proportional to the square root of pump field density), and $\Delta\nu_{\mathrm{FIR}}$ is proportional to pump power density.

Because there is noticeable uncertainty in published values for dipole matrix elements (50), and considerable inaccuracy in estimating the circulating pump intensity (41), β is best estimated from a combination of a model for circulating pump field (see section entitled "Physical Theory") (35), and experimental data.

The results of the TPLS modeling of the 118.83 μm line, with operational parameters commensurate for the NASA CHEM 1 system (23), are presented in Figs. 13 and 14. As shown there the expected TPLS is the 60 kHz worst case @ 1 MHz of pump dither, and the TPLS can be minimized by operating the pump laser only slightly off of the vibrational line center. In a standing-wave OPSL the maximum efficiency point will naturally be off line center.

Amplitude Stability. High-amplitude stability operation of OPSLs requires careful attention to a number of design criteria. The present article will concentrate on some of the more dominant ones: (1) inherent pump laser stability, (2) pump-laser feedback, (3) inherent SMMW laser cell stability, and (4) SMMW feedback. While this list certainly does not cover all of the issues, it does illustrate some of the major points.

1. *Inherent Pump Laser Stability.* The pump laser stability can be broken down into three major areas: mode purity and stability, frequency stability, and amplitude stability. For the purposes of this discussion, consider the pump laser to be isolated from the SMMW laser, and thus only consider its "independent" properties. The pump laser's frequency stability will affect the OPSL's amplitude stability through modulation of the percentage of pump radiation absorbed (the frequency dependence of the pump transition) and through modulation of the OPSL operating frequency (the amplitude-frequency tuning of the SMMW transition). As indicated in the preceding section, these effects may be quite complex to evaluate numerically; however, in general, stable OPSL operation requires the pump frequency to remain fixed to better than ~5 MHz.

   The pump laser's spatial mode purity and spatial mode stability are often related in that a single mode pump laser will, by definition, only operate on one mode. Therefore its mode stability is assured. Mode changes in the pump laser induce amplitude changes in the SMMW laser output through time variation of the pump field distribution within the SMMW cavity. Thus the highest degree of amplitude stability demands mode stability, and single-mode pump operation is desirable. The other consideration for mode purity is efficiency. If the pump laser is emitting more than one frequency, it will be a less effective pump, because it will pump velocity groups other than the desired set.

   Amplitude variations in the pump laser couple into the SMMW laser almost linearly. Therefore if the pump laser's amplitude is only stable to 10%, the SMMW output will only be stable to 10%.

2. *Pump-Laser Feedback.* This topic is of great concern for stable operation. Since there are presently no practical high-power isolators for CO_2 lasers, pump laser feedback from the SMMW cavity back into the pump laser cavity is a serious issue (with the exception of a circular-polarization isolator, which has the unfortunate property of affecting the output polarization of the OPSL and decreasing its efficiency). While a high-band-

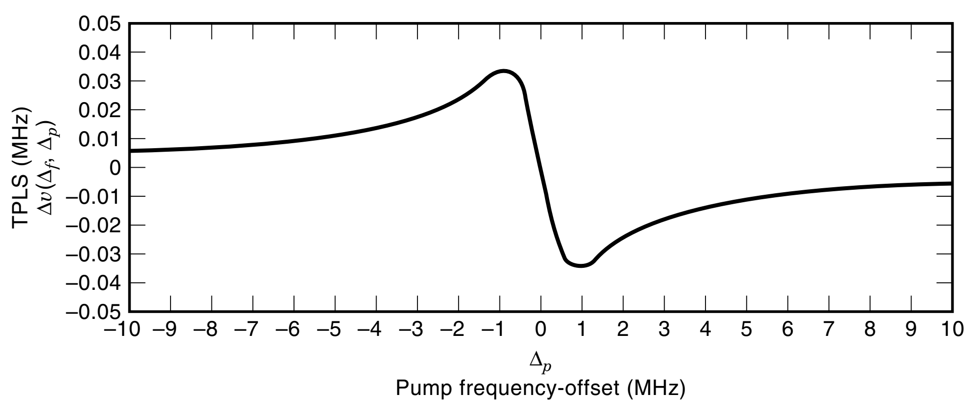

Figure 13. Two-photon light shift versus pump offset.

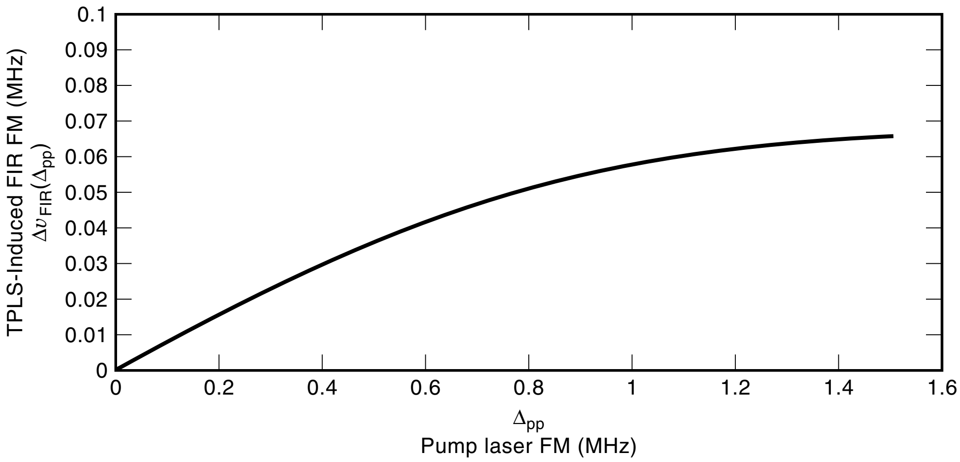

Figure 14. Worst-case two-photon light shift versus pump dither amplitude.

width frequency lock can keep the pump laser at the desired operating frequency, it cannot compensate for the change in apparent output coupler reflectivity.

For illustration, first consider a single-mode pump laser. In this case the output coupler and feedback source can be thought of as a Fabry–Perot output coupler. The reflectivity of such a device is not only a function of the reflectivity of the output coupler and feedback coupling, but also a function of the absolute distance between the effective feedback source and the output coupler. [See Eqs. (15) and (16), later in this section.] In fact the reflectivity will go through a complete cycle for every $\lambda/2$ change in distance. With pump wavelengths in the 10 μm range, and the thermal expansion coefficients of typical optical table materials ($\sim 10 \times 10^{-6}$ C^{-1}), one can expect substantial changes in effective reflectivity with even moderate changes in environmental temperature. Since the pump laser will have an output which varies with output coupling, its amplitude will vary with temperature. This will induce similar changes in SMMW output power.

By operating the pump laser in a coupled-cavity mode, where both end mirrors can be moved, feedback effects can be mitigated (with suitable control electronics). This approach effectively treats the feedback as a part of the pump laser cavity, working with it. It should be noted that pump feedback can also be reduced by (1) coupling into the SMMW cell with as fast an optic as practical (still wishing to maintain efficiency, which unfortunately optimizes for slow input coupling optics) to allow reduced input hole sizes (2 mm is a typical input coupling hole diameter) and to effectively "scramble" the pump field, (2) employing an off-axis input coupling hole, or (3) constructing a SMMW ring laser (to completely eliminate pump feedback).

The effects of pump feedback for a multimode pump laser are much more complicated. In that case, not only are the processes discussed above in effect, the pump laser may also shift transverse modes. To understand this, consider a multimode pump laser in the presence of external feedback. The feedback enters the cavity with a phase which is different than that of the circulating radiation already within the cavity. This feedback radiation will induce stimulated emission at the "wrong" phase, depleting the gain of the operating mode. At some point the gain of another transverse mode may exceed the gain of the desired mode, causing a change in pump laser spatial mode structure and, hence, a commensurate change in SMMW output amplitude. At that point the process may start again. Many times such a system will be seen to operate in a "bistable" fashion, operating at one output level and then quickly switching to another and back. While all of this might make it sound like building an OPSL with a multimode pump laser is folly, this is not the case. A number of well-behaved OPSL systems employing multimode pump lasers have been constructed over the years, and in fact only in recent years, with the advent of modest cost true waveguide CO_2 lasers, has construction of single-mode-pumped OPSLs become practical.

3. *Inherent SMMW Laser Cell Stability.* Inherent SMMW Laser Cell Stability - The inherent cell stability can be broken into two main areas: mechanical stability and vacuum integrity. For long-term amplitude and frequency stability, the SMMW laser structure must hold the end mirrors in their correct positions through both temperature changes and vibrations.

The precision with which the length must be maintained is quite impressive. If one takes an example of an SMMW laser with a cavity length of 1.5 m, operating at a wavelength of 200 μm and assuming that the FWHM of the SMMW lasing is 10 MHz, then the SMMW laser will only provide output over a range of $\sim$14 μm every 100 μm. Outside of this range the laser either will have no output or will output at higher-order transverse modes or other lines. Thus optimization of the output requires submicron-length translation resolution; and since the output amplitude is a function of the operating frequency, maintaining a specified amplitude requires submicron mirror-spacing stability.

The vacuum integrity of the OPSL is also paramount for long-term, stable operation. If the OPSL's vacuum integrity is not sufficient to permit sealed-off operation, then a vacuum pump must be operated and the OPSL gas flowed. If pump vibrations [even very slight vibrations; see Eq. (12)] are allowed to mechanically couple into the OPSL cell, then amplitude and frequency varia-

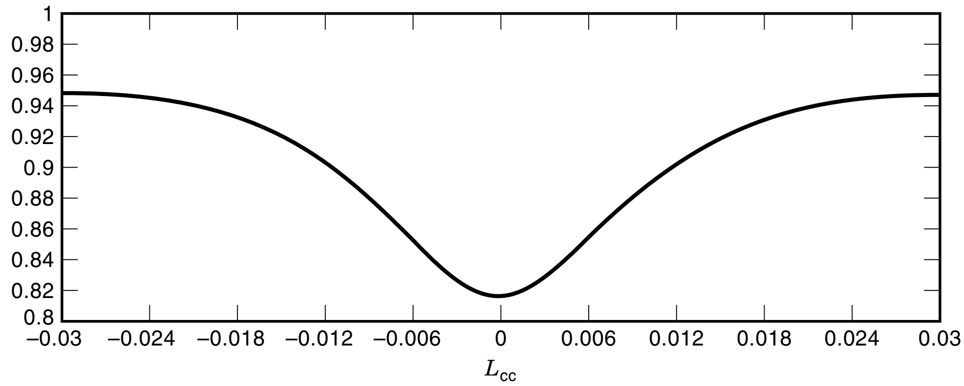

Figure 15. Effective output coupler reflectivity versus L_{fb} for $\lambda = 118.83\ \mu$m, $R_{oc} = 90\%$, and $R_{fb} = 10\%$. The horizontal axis is in millimeters and therefore goes from $-30\ \mu$m to 30 μm. The vertical axis is reflectivity.

tions will result. Furthermore, the flowing gas system is a ready source of contamination. Sealed-off operation is a very desirable feature.

4. *SMMW Feedback.* The issue of SMMW feedback can be broken into three main topics: two-photon light shift, feedback-induced frequency pulling, and feedback-induced output reflectivity pulling. The first of these can be avoided by choosing a ring-resonator configuration (30), and can be minimized by operation of the pump laser off of the vibrational line center. A simple way to evaluate the other two is to view the output coupler and SMMW feedback source as a Fabry–Perot output coupler.

The effective reflectivity of a lossless Fabry–Perot etalon output coupler is given by

$$R = \left| \sqrt{R_{oc}} - \frac{e^{-i4\pi^{L_{fb}/\lambda}}(1-R_{oc})\sqrt{R_{fb}}}{1-\sqrt{R_{oc}R_{fb}}e^{-i4\pi^{L_{fb}/\lambda}}} \right|^2 \tag{15}$$

and the effective phase seen by the cavity at the etalon face is given by

$$\varphi = \arg\left[\sqrt{R_{oc}} - \frac{e^{-i4\pi^{L_{fb}/\lambda}}(1-R_{oc})\sqrt{R_{fb}}}{1-\sqrt{R_{oc}R_{fb}}e^{-i4\pi^{L_{fb}/\lambda}}} \right] \tag{16}$$

where L_{fb} is the distance between the output coupler and the feedback source, R_{oc} is the reflectivity of the isolated output coupler, R_{fb} is the effective reflectivity of the feedback source, and λ is the operating wavelength of the laser.

First examining Eq. (15), one can see how SMMW feedback will affect the amplitude stability of the OPSL. A plot of effective reflectivity versus L_{fb} is presented in Fig. 15. As demonstrated there, the feedback in this typical example pulls the effective reflectivity from a maximum 94.5% to a minimum of 81%. This pattern repeats itself for every $\lambda/2$ change in distance between the feedback source and the output coupler. Since the output power will be a function of output coupler reflectivity (see Fig. 12), the output amplitude of the OPSL will modulate with small changes in L_{fb}. This effect is expected to be reduced in ring-resonator OPSLs. However, ring-resonator OPSLs may suffer direction switching induced by feedback, depending on pump conditions.

With Eq. (16), the feedback-induced frequency pulling can be calculated as

$$\Delta\nu \approx \frac{c\varphi}{2\pi L_c} \tag{17}$$

where c is the speed of light, ϕ is given by Eq. (16), and L_c is the OPSL's nominal cavity length. A plot of Eq. (17), for the same conditions of Fig. 15, is presented in Fig. 16. The feedback in this example can pull the output frequency of the OPSL by a total of more than 2 MHz. This may not be acceptable in many applications.

Both of the output coupling effects described above can be controlled with an appropriate control loop (23) or their effects can be stabilized through the use of very rigid and thermally stable structures/environments.

AN EXAMPLE OPSL SYSTEM: THE NASA CHEM 1 SATELLITE, 2.5 THz LASER LOCAL OSCILLATOR

Introduction

In order to provide a global mapping of OH (and also O_2), the Microwave Limb Sounder (MLS) on the CHEM I satellite, to be launched in 2002, will have channels with a local oscillator (LO) at 2.52 THz (these channels will be collectively referred to as the THz channel). The LO for the THz channel is a methanol laser pumped by a CO_2 laser.

The THz channel is one of five radiometer channels on the MLS. While DeMaria ElectroOptics Systems (DEOS) is providing the Laser Local Oscillator (LLO) system for the THz

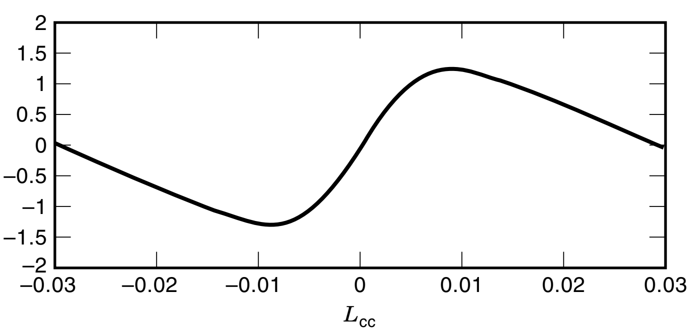

Figure 16. Feedback-induced SMMW frequency pulling. The horizontal axis is in mm, and the vertical axis is the feedback-induced frequency pulling in MHz.

channel, NASA's Jet Propulsion Laboratory (JPL) is fabricating the receivers, performing the systems integration, and conducting the atmospheric data evaluation.

The LLO is a high-reliability system which uses a combination of existing and new laser technologies. Starting with the pump laser technology, the LLO will utilize the same high-reliability, sealed-off, RF-excited, CO_2 laser technology found in sealed-off, RF-excited, industrial CO_2 lasers and in numerous high-sophistication CO_2 laser systems delivered and fielded over the years. Specifically, this technology has demonstrated operating life in excess of 35,000 h, shelf life of over 10 years, operation in high-performance aircraft environments, spectral purity and stability sufficient for LIDAR applications, and all within a very compact and rugged package.

Applicable vacuum and optical techniques from the CO_2 laser design are incorporated into the SMMW laser design. Thus while ultra-high-stability and spectral purity SMMW lasers which have operated for years with only periodic gas refills have been constructed in the past, the sealing and mirror mount technologies adopted from the CO_2 laser designs are expected to yield SMMW lasers which operate for years *without* refilling or service of any kind.

In the design of a system as intricate, efficient, and autonomous as the LLO, a number of complex interactions, which may not be imperative for a laboratory-based system, must be considered to assure a robust design. The remainder of this section will present the LLO design, with limited details, in the subsections that follow: "LLO Specifications," "LLO Configuration," "High-Efficiency Pump Laser," "Pump Laser Frequency Control," and "The SMMW Laser."

LLO Specifications. The LLO has a long list of specifications. In the interest of brevity, only those specifications which relate to topics covered in this section will be presented.

The LLO must autonomously operate and produce sufficient output power to optimize two Schottky diode receivers. The output power specification is 20 mW. The required lifetime is 5 years on-orbit plus 2200 h of ground testing. All specifications are required to be met over the entire lifetime of the LLO and thus constitute the definition of lifetime.

There are significant constraints on available prime power, mass, and envelope. The entire LLO (including all control electronics) must fit in a box no larger than $75 \times 30 \times 10$ cm. The allowed total mass is 20 kg, and the total available 28 V direct-current (dc) prime power is 120 W. The size/mass/efficiency portion of the specification drives a large part of the LLO design.

Further mechanical constraints are in force via the launch survival specification. While the LLO does not have to operate during launch, it must of course survive launch. With the LLO's position on the Delta II launch vehicle, this amounts to 14.1 g root mean square (rms) for 1 min on all three axes. Furthermore, with the launch platform's acceleration profile, the time from atmospheric pressure to 1 torr is $\sim$30 s. Therefore adequate venting must be provided to prevent rupture of nonpressure enclosures.

The frequency stability requirements are (1) 100 kHz/s (full width at half-maximum), long-term drift not to exceed 2 MHz from line center, and (2) spectral purity-sidebands <-30 dBc ($>$200 kHz off carrier). Since a SuperInvar structure would not be compatible with the mass budget, a novel method of active frequency control for the SMMW laser has been devised (23).

The required amplitude stability is 1% over 30 s. System level Rigrod modeling has shown this to be dominated by feedback interaction with the diplexer/receiver system. DEOS has devised a novel method to mitigate this effect as well.

The output spatial mode specification is that only power in the specified TEM_{00} mode is counted, and the LLO output beam waist must be 4.1 mm located 465 mm from the LLO–radiator interface.

The output polarization specification is equal parts horizontal and vertical (within 10%) with any phase relationship. Thus circular polarization or 45° linear polarization is acceptable; 45° linear is the baseline for the LLO.

All of the performance specifications must be met in the presence of feedback from the diplexer/receivers. This is expected to be less than 20%. Accordingly the specification is robustness to up to 20% SMMW feedback of arbitrary phase and polarization. A method to mitigate the SMMW feedback has also been devised (23).

The temperature range specification for the LLO is nontrivial as well. The system will be tested from -10 to 50°C (operational), and from -35°C to 60°C (nonoperational survival).

LLO Configuration. The LLO block diagram is shown in Fig. 17. The LLO electronically interfaces with the MLS via three main connections: prime power, RS-422 communications, and mixer bias signal.

To illustrate the operation of the LLO, "follow the power." Prime power is converted into radio-frequency (RF) power in the RF power supply. The RF power propagates through coaxial hard-line to the pump laser and excites the Pump Laser. The emitted 9.69 μm light propagates through the pump beam delivery optics and photoacoustic cell into the SMMW laser. Included in the pump beam optics are beam sample optics which send a very small portion of the pump power into a frequency amplitude control pyro and health-and-status thermopile. The SMMW laser converts the pump light to SMMW light at 118.83 μm (2.52 THz). Finally the SMMW beam delivery optics transform the laser output mode to match the specified output profile.

A drawing of the LLO is presented in Fig. 18. The control/interface electronics reside in the upper portion of the housing (control/interface electronics unit), and the RF power supply and all optical components are located in the lower portion of the housing (electrooptic unit). A radiator plate is mounted to the electrooptic unit and radiates the waste heat created by the LLO. The radiator is not structural; in fact the LLO provides the support for the radiator. The LLOs mechanical interface with the MLS is through three bipod struts (not shown) which mount to tabs shown in Fig. 19.

The optical path for the LLO is presented in Fig. 19. As shown there, the available space is quite constrained. The pump beam propagates through the photoacoustic cell (PA cell) and then through the lens which focuses the beam into the SMMW laser. Using crossed-Brewster pairs to "pick-off" small portions of the pump beam, beam samples are sent to the pyroelectric detector (which is used by the pump laser frequency/amplitude control electronics) and to the thermopile (pump power, health, and status). Provision has been made for a $\frac{1}{4}\lambda$ plate, if more pump isolation is required.

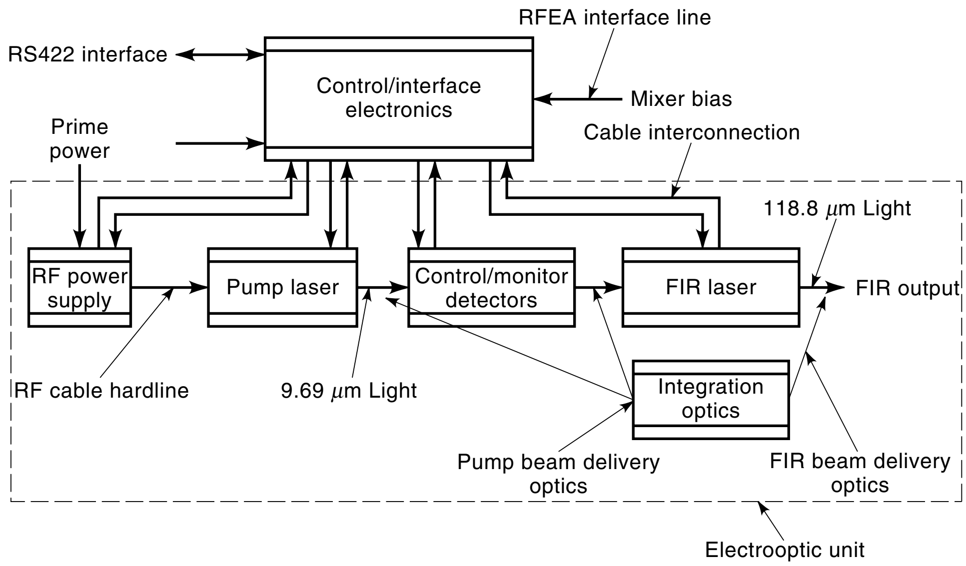

Figure 17. Block diagram of LLO.

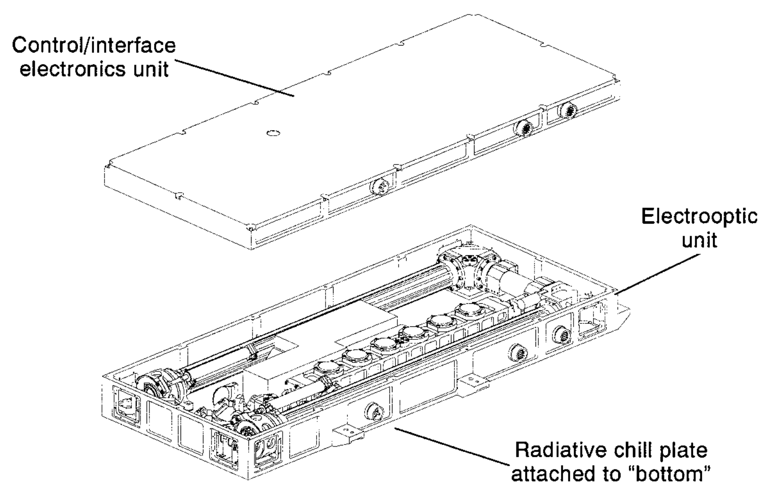

Figure 18. LLO system, enclosure opened.

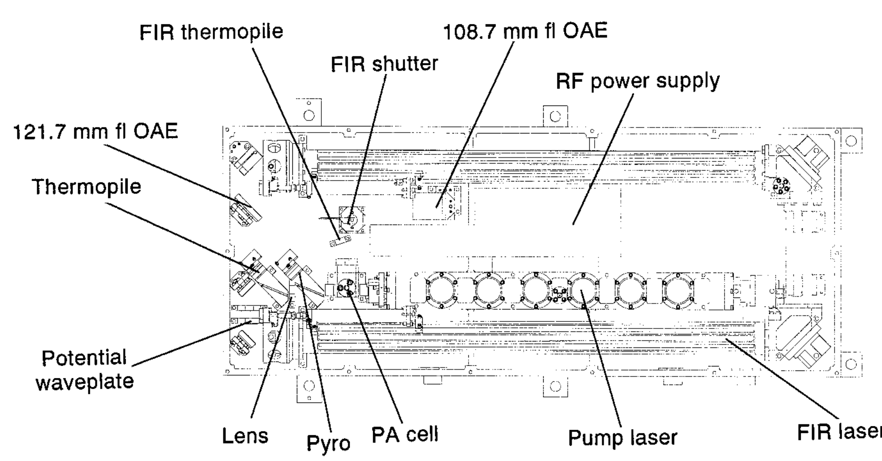

Figure 19. LLO optical path.

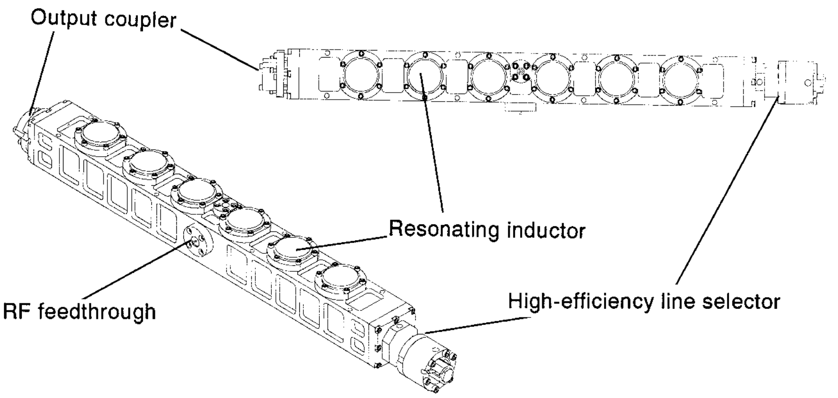

Figure 20. High-efficiency pump laser.

The output from the SMMW laser will be transformed to match the specified beam profile via a Newtonian telescope. This telescope is formed by two off-axis elliptical mirrors. The fastest *f*# in the telescope is ~7. The mirrors will be diamond-turned Al, fabricated in conjunction with their respective optical mounts.

The SMMW shutter is included to prevent a gain-switched SMMW spike, possible during initial turn-on, from damaging the receivers. (Note that if conditions are right, the pump laser can put out a ~500 W pulse at turn-on.) The back of the shutter is mirrored, so that when the shutter is closed the SMMW beam will propagate into the SMMW thermopile (health and status). As the output telescope for the SMMW beam is Newtonian, the focal spot from the telescope is an ideal location for coupling into the thermopile. This obviates the need for an additional SMMW focusing element in front of the SMMW thermopile detector.

High-Efficiency Pump Laser. The first requirement for a high-efficiency pump laser is a high-efficiency RF power supply. In preparation for the LLO program a high-efficiency power supply was constructed. This supply demonstrated 75 W of RF out with 100 W of dc in. The RF power supply is a conductively cooled device that uses a class-C power amplifier stage.

Effective use of the available RF power is also key to high-efficiency operation. Through a number of patented techniques, DeMaria ElectroOptics Systems (DEOS) is able to very efficiently couple the RF power into the discharge.

Diagrams of the high-efficiency pump laser are shown in Fig. 20. This laser is very compact and low in mass (~1.5 kg). The RF circuit of the laser is formed by the combination of the electrode/waveguide/enclosure capacitance and the resonating inductors. The RF power is admitted through a RF feedthrough in the side of the laser. The cavity is formed by the output coupler, on one end, and the high-efficiency line selector, on the other. This line selector greatly increases the efficiency of the laser, since it has an effective reflectivity at 9.69 μm of >99%.

As with the entire LLO project, extensive mathematical modeling of the pump laser has been utilized. In particular, DEOS has measured Rigrod parameters for a complete distributed-loss Rigrod model (42) of the pump laser. Based on this model, it appears that the pump laser will have an output power of ~10 W at delivery. (In a demonstration program, DEOS delivered a first-generation integrated pump laser/RFPS which had an output power of >9 W @ 9P36 with 100 W of DC input.)

Pump Laser Frequency Control. Precise control of the pump frequency is essential for the LLO to meet all specifications. During the demonstration program the effects of operating the pump laser at its line center were studied, since this could significantly simplify the frequency control. However, it was found that operation at 9.69 μm line center causes a 2 dB loss in SMMW efficiency. Therefore it was decided that this would not be acceptable.

Another possible frequency control scheme would involve trying to lock the pump frequency by observing the SMMW output. Careful analysis and modeling showed this to be a poor approach, entangling numerous physical effects and making the frequency control nonrobust at best.

To obtain an absolute frequency reference to lock the pump laser against, a photoacoustic cell (see Fig. 21) which uses the SMMW laser vibrational pump transition in methanol (51), was designed and tested.

The PA cell is a very simple device. Essentially it is a sealed cavity which contains methanol at ~500 mtorr, a pre-polarized microphone, and AR windows.

The physical basis for the PA cell-based pump frequency locking method is presented graphically in Fig. 22. The pump laser is dithered about a portion of the methanol vibrational absorption line, producing an acoustic signal as the amount of absorbed power is modulated. The pressure of the cell is set to be low enough that no more than 200 mW of pump power is absorbed.

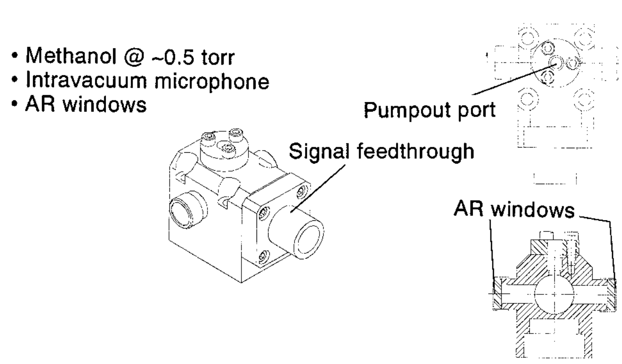

Figure 21. Photoacoustic molecular frequency standard.

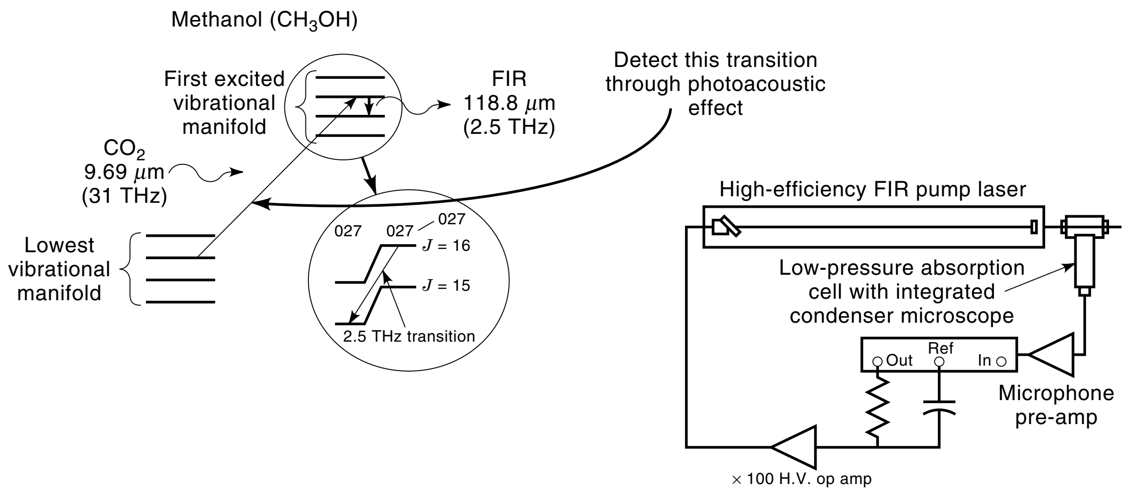

Figure 22. Pump-laser frequency locking method.

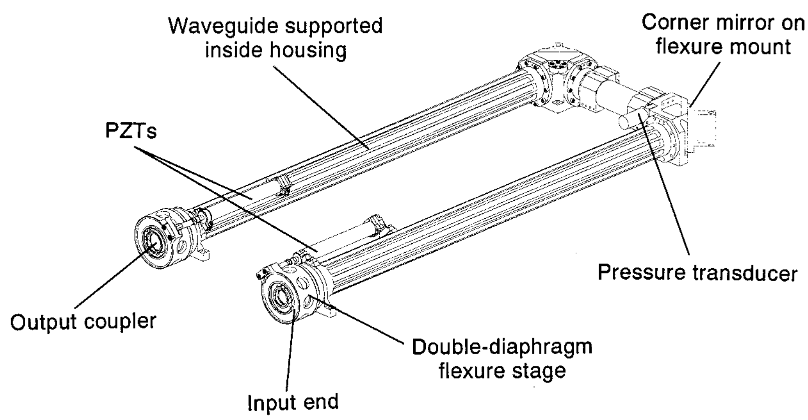

Figure 23. Standing-wave SMMW laser.

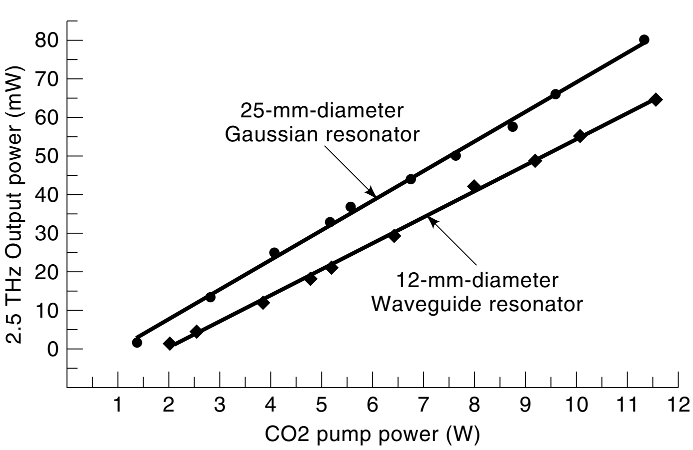

Figure 24. The 1.5 m straight-guide demonstration program SMMW results.

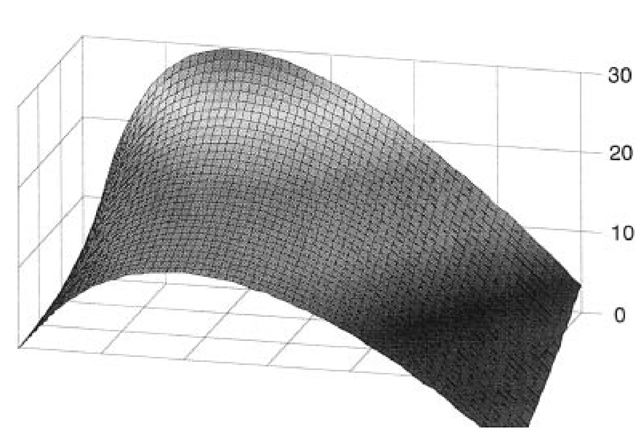

Figure 25. Rigrod prediction for SMMW output versus turn loss and output coupling. Pump power fixed at 5 W.

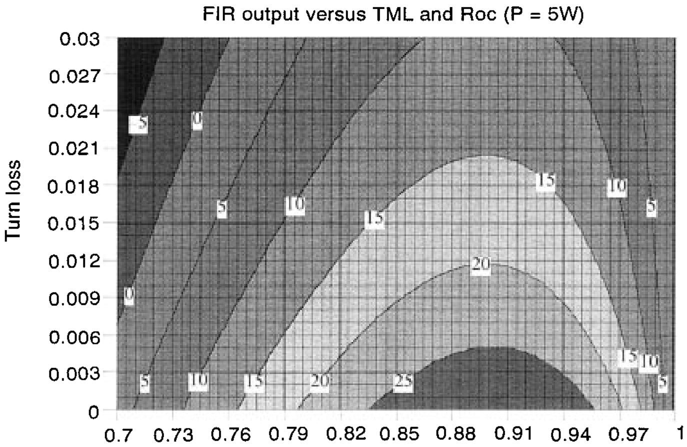

Figure 26. Rigrod prediction for SMMW output versus turn loss and output coupling (plan view of Fig. 25). Pump power fixed at 5 W.

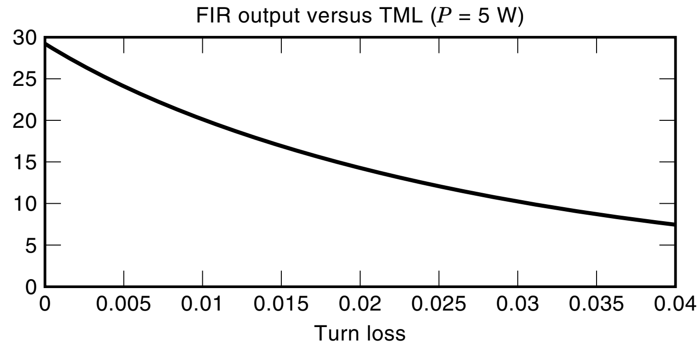

Figure 27. Rigrod prediction for SMMW output (mW) versus turn loss. Output coupling fixed at 9%, pump power fixed at 5 W.

While the pump laser FM will couple into the SMMW output spectrum, this effect should be due to primarily two sources. The first of these, Doppler coupling induced by velocity memory effects, was described in the section entitled "Frequency Stability and Laser Tune-up." With the parameters for the LLO's SMMW laser, the Doppler-coupling factor is $\sim\frac{1}{12}$. Therefore the induced SMMW dither will be down by a factor of 12 with respect to the pump dither. Because this technique has already been demonstrated with <1 MHz of pump dither, this does not appear to be a problem with respect to the 100 kHz short-term frequency noise specification.

The above does not exhaust sources of frequency noise induced by this locking technique. There is also the two-photon light shift described in the section entitled "Frequency Stability and Laser Tune-up" (46). While the model presented there is not complete, it does give good agreement with the measured results for other SMMW lines and predicts a <60 kHz effect here. There do not appear to be any direct measurements of the TPLS for the 2.52 THz line, but Plainchamp (52) has indicated that the TPLS appears to be anomalously small for this transition.

The SMMW Laser. For reasons of risk (30) and schedule, the option of a ring SMMW laser was dropped from the LLO early in the program. A drawing of the standing-wave SMMW laser for the LLO is shown in Fig. 23.

Both the input and output mirrors are mounted on lead-zirconate-titanate piezotranslator (PZT)-actuated flexure stages. The corner mirrors are mounted on diaphragm flexure alignment mounts. The housing is aluminum with the dielectric waveguides supported inside with flexible wavesprings.

The input coupler and turn mirrors are diamond-turned copper and the input coupling is through a hole in the input mirror. The output coupler is a uniform capacitive mesh-type coupler (20). Modeling of the mesh output couplers was accomplished using the GLAYERS program of CSIRO (32).

Both the modeling and the demonstration program results showed optimal uniform output coupling to be necessary to achieve high-efficiency operation. Some of the output power versus pump power results obtained during the demonstration program are presented in Fig. 24. All of these data were obtained with the pressure held fixed at the optimal pressure for 5 W of pump power, to more accurately simulate flight conditions (i.e., once sealed the SMMW pressure cannot be adjusted, and therefore optimization at the low end of pump power is prudent). The results in Fig. 24 bracket the cavity geometries required to meet the initial internal goal of 20 mW out with 5 W of pump power. In looking at Fig. 24, it should be remembered that the delivered pump laser actually had an output power of >9 W; thus a great deal of margin was demonstrated.

The results of Fig. 24 are for a straight-guide laser, and the losses associated with cavity turns are expected to reduce

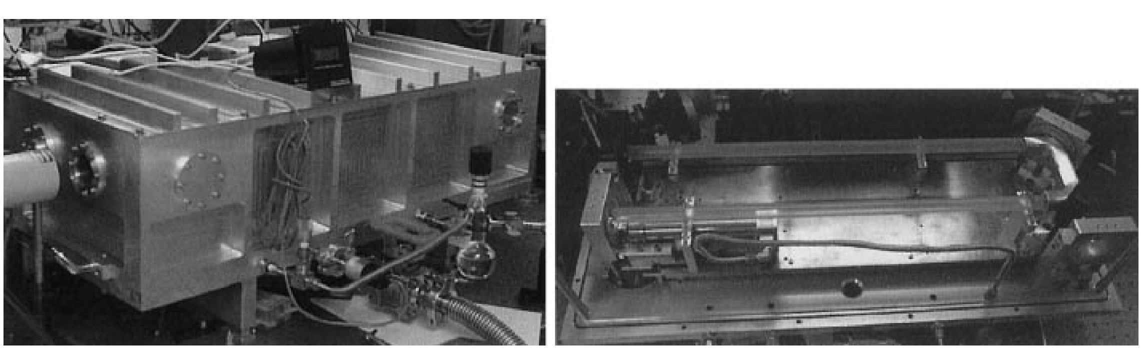

(a) (b)

Figure 28. SMMW testbed laser. (a) External view, (b) internal view.

efficiency and improve mode selection. DEOS developed a distributed-loss Rigrod model, a reformation of Eq. (10), for the SMMW laser including the effects of turn losses. The results of this model with 5 W of pump power are summarized in Figs. 25, 26, and 27.

Figures 25 and 26 plot the output power versus output coupling and turn loss, with the pump power fixed at 5 W. Figure 27 presents the output power versus turn loss with the output coupling fixed at 9% and the pump power fixed at 5 W.

All of the parameters for the Rigrod model were determined experimentally during the demonstration program. There were no adjustable parameters at this stage of the modeling effort. The most important conclusion of these figures is that turn loss is the key to high-efficiency operation. The LLO's SMMW laser operates in the low-gain low-loss regime; thus any loss is significant. Although not shown in this section, the experimental results for a folded SMMW laser show the threshold regime to be below 5 W of pump power; thus the LLO's SMMW laser will be operating above the threshold regime.

To test the SMMW models, and then later to improve them, a high-versatility testbed laser was constructed. Figure 28 shows the external and internal view of the testbed laser. The testbed is an aluminum enclosure housing a SuperInvar plate on which all of the optical stages are mounted. Cavity translation is accomplished via a 180 μm travel PZT. A wide range of waveguide diameters can be used in this laser and easily changed, since they are not involved in the vacuum seal.

The testbed laser also has two ports at each corner to enable virtually any cavity configuration. The three guide pieces are held together in a precision miter, and they are supported in precision-machined V-blocks and restrained by standard coil springs stretched across the guide sections. All four of the gimbal stages are slightly modified commercial units.

The results obtained with the testbed laser are presented in Fig. 29 along with a comparison to the original model results obtained. As observed in there, the experimental results are within 9% of the original prediction. This prediction was based on an estimate for the turn loss of 0.8%/turn (reflectivity loss + guide–guide loss around the turn as a result of the unguided region of the mitered corner). If one now takes the Rigrod model and treats the turn loss as an adjustable parameter, then with a turn loss of 1.2%/turn and including the efficiency variation with pump power, the model falls directly over the experimental data.

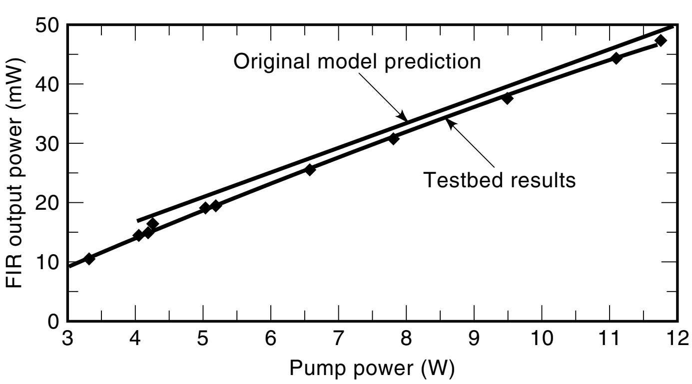

Figure 29. Testbed results: Comparison with original model.

BIBLIOGRAPHY

1. T. Y. Chang and T. J. Bridges, Laser action at 452, 496, and 541 μm in optically-pumped CH_3F, *Opt. Commun.,* **1** (9): 423, 1970.
2. J. Burghoorn et al., Generation of subnanosecond high-power far-infrared pulses by using a passive resonator pumped by a free-electron laser, *J. Opt. Soc. Amer.,* **9**: 1888, 1992.
3. K. Unterrainer et al., Tunable cyclotron-resonance laser in germanium, *Phys. Rev. Lett.,* **64**: 2277, 1990.
4. C. T. Gross et al., Pulsed high-power far-infrared gas lasers: Performance and spectral survey, *IEEE J. Quantum Electron.,* **23**: 377, 1987.
5. T. E. Wilson, in R. LeChevalier (ed.), *Summary Report of the New and Innovative Concepts Program of the US Department of Energy,* Falls Church, VA: TPI, 1989, p. 79; T. E. Wilson, A high-power far-infrared NH_3 laser pumped in a three-mirror CO_2 laser cavity with optically-switched cavity-dumping, *Int. J. Infrared Millim. Waves,* **14**: 303, 1993; R. E. M. de Bekker, L. M. Classen, and P. Wyder, Generation of very short far-infrared pulses by cavity dumping a molecular gas laser, *J. Appl. Phys.,* **68**: 3729, 1990.
6. H. R. Fetterman et al., Submillimeter heterodyne detection of interstellar carbon monoxide at 434 micrometers, *Science,* **211**: 580, 1981; G. A. Koepf, et al., CO ($J = 6 \rightarrow 5$) distribution in Orion and detection in other galactic sources, *Astrophys. J.,* **265**: 824, 1982.
7. G. Chin, Optically pumped submillimeter laser heterodyne receivers: Astrophysical observations and recent technical developments, *Proc. IEEE,* **80**: 1788, 1992.
8. G. E. Stillman et al., Precision verification of effective mass theory for shallow donors in GaAs, *Solid State Commun.,* **9**: 2245, 1971; H. R. Fetterman, et al., Identification of donor species in high-purity GaAs using optically pumped submillimeter lasers, *Appl. Phys. Lett.,* **21**: 434, 1972.
9. E. R. Mueller et al., Definitive identification of D^- centers in GaAs quantum wells by tilt-induced line splitting in a magnetic field, *Phys. Rev. Lett.,* **68**: 2204, 1992.
10. G. J. Simonis, Index to the literature dealing with the near-millimeter wave properties of materials, *Int. J. Infrared Millim. Waves,* **3**: 439, 1982.
11. A. J. Cantor et al., Application of submillimeter wave lasers to high voltage cable inspection, *IEEE J. Quantum Electron.,* **QE-17**: 477, 1981.
12. T. Y. Chang, T. J. Bridges, and E. G. Burkhardt, cw submillimeter laser action in optically-pumped methyl fluoride, methyl alcohol, and vinyl chloride gases, *Appl. Phys. Lett.,* **17**: 249, 1970.
13. H. A. Gebbie, N. W. B. Stone, and F. D. Findlay, *Nature,* **202**: 685, 1964.
14. H. R. Fetterman et al., Far-IR heterodyne radiometric measurements with quasioptical Schottky diode mixers, *Appl. Phys. Lett.,* **33**: 151, 1978.
15. D. D. Bicanic, B. F. J. Zuidberg, and A. Dymanus, Generation of continuously tunable laser sidebands in the submillimeter region, *Appl. Phys. Lett.,* **32**: 367, 1978.
16. E. R. Mueller and J. Waldman, Power and spatial mode measurements of sideband generated, spatially filtered, submillimeter radiation, *IEEE Trans. Microw. Theory Tech.,* **42**: 1891, 1994.
17. D. T. Hodges, A review of optically pumped far-infrared lasers, *Infrared Phys.,* **18**: 375, 1978.
18. M. S. Tobin, A review of optically pumped NMMW lasers, *Proc. IEEE,* **73**: 61, 1985.
19. S. Jacobsson, Review, optically pumped far infrared lasers, *Infrared Phys.,* **29**: 853, 1989.
20. R. Densing et al., Effective far-infrared laser operation with mesh couplers, *Infrared Phys.,* **33**: 219, 1992.

21. J. M. Manley and H. E. Rowe, Some general properties of nonlinear elements. Part 1. General energy relations, *Proc. IRE,* **44**: 904, 1956.
22. J. Farhoomand and H. M. Pickett, Stable 1.25 watts cw far infrared laser radiation at the 119 μm methanol line, *Int. J. Infrared Millim. Waves,* **8**: 441, 1987.
23. E. R. Mueller et al., 2.5 Thz laser local oscillator for the EOS chem 1 satellite, *Proc. 9th Int. Symp. Space Terahertz Technol.,* pp. 563–572, 1998.
24. L. A. Newman and R. A. Hart, Recent R&D advances in sealed-off CO_2 lasers, *Laser Focus/Electro-Opt.,* **23**: 80–91, 1987.
25. W. J. Weber (ed.), *CRC Handbook of Laser Science and Technology,* Vol. 2: Gas lasers, Boca Raton, FL: CRC Press, 1982.
26. M. Rosenbluh, R. J. Temkin, and K. J. Button, Submillimeter laser wavelength tables, *Appl. Opt.,* **15**: 2635, 1976.
26a. M. Inguseio et al., A review of frequency measurements of optically pumped lasers from 0.1 to 8 THz, *J. Appl. Phys.,* **60**: R161–R192, 1986.
27. G. M. R. S. Luis et al., Observation and characterization of new FIR lines from formic acid, *IEEE J. Quantum Electron.,* **34**: 767, 1998.
28. J. Waldman et al., Submillimeter modeling of millimeter radar systems, *SPIE,* **259**: 152, 1980.
29. S. K. Kim, D. L. Brower, and N. C. Luhmann, Experimental measurement of electron particle diffusion from sawtooth-induced density-pulse propagation in the Texas experimental tokamak, *Phys. Rev. Lett.,* **60**: 577, 1988.
30. J. H. Lee et al., Development of a far-infrared ring laser for plasma diagnostic applications, *Rec. Sci. Instrum.,* **63** (10): 4678, 1992.
31. H. P. Roser et al., Investigations of optically pumped submillimeter wave laser modes, *Int. J. Infrared Millim. Waves,* **3** (6): 839, 1982.
32. P. A. Stimson and L. B. Whitbourn, *GLAYERS, A Program for the IBM PC which Calculates the Properties of Metal Grids in Dielectric Stacks,* 1989.
33. T. A. De Temple and E. J. Danielewicz, Continuous-wave CH_3 waveguide laser at 496 μm: Theory and experiment, *IEEE J. Quantum Electron.,* **QE-12**: 40, 1976.
34. J. O. Henningsen and H. G. Jensen, The optically pumped far-infrared laser: Rate equations and diagnostic experiments, *IEEE J. Quantum Electron.,* **QE-11**: 248, 1975.
35. J.-M. Lourtioz and R. Adde, Diagnostic experiments and modeling of the 118 μm CH_3OH laser, *J. Phys. (Paris),* **41**: 251, 1980.
36. E. R. Mueller et al., Generation of high repetition rate far-infrared laser pulses, *Appl. Phys. Lett.,* **64**: 3383, 1994.
37. Data taken from the DeMaria ElectroOptic Systems LLO Demonstration Program final report.
38. J. R. Tucker, *Int. Conf. Submillim. Waves Their Appl.,* Atlanta, GA, 1974, p. 17.
39. J. O. Henningsen, Assignment of laser lines in optically pumped CH_3OH, *IEEE J. Quantum Electron.,* **QE-13**: 435, 1977.
40. E. V. Ivash, J. C. M. Li, and K. S. Pfitzer, *J. Chem. Phys.,* **23**: 1814, 1955.
41. A. Harth, Pump beam propagation in circular waveguides of optically pumped far-infrared lasers, *Int. J. Infrared Millim. Waves,* **12**: 221, 1991.
42. W. W. Rigrod, Homogeneously broadened CW lasers with uniform distributed loss, *IEEE J. Quantum Electron.,* **QE-14**: 377, 1978.
43. R. L. Crownover et al., Frequency stability and reproducibility of optically pumped far-infrared lasers, *Appl. Phys. Lett.,* **57**: 2882, 1990.
44. A. Yariv, *Optical Electronics,* 4th ed., Chicago: Holt, Rinehart & Winston, 1991, p. 383.
45. R. I. McCormick, F. C. DeLucia, and D. D. Skatrud, Collisional energy transfer in optically pumped far-infrared lasers, *IEEE J. Quantum Electron.,* **23**: 2609, 1987.
45a. The reader may note that in general the pump field will interact with two velocity groups in a standing-wave laser: One group will move at the correct velocity toward the input end, while the corresponding group will move away.
46. C. R. Pidgeon et al., Two-photon light shift and Autler–Townes splitting in optically pumped FIR lasers, *Int. J. Infrared Millim. Waves,* **2** (2): 207, 1981; see also Ref. 49.
47. DeMaria ElectroOptics Systems is developing a high-power, autonomous SMMW laser system for Goddard Space Flight Center, to be used on an observation aircraft. This system will have an "all" wavelength absolute pump-frequency lock.
48. S. H. Autler and C. H. Townes, Stark effect in rapidly varying fields, *Phys. Rev.,* **100**: 703, 1955.
49. S. T. Shanahan and N. R. Heckenberg, Heterodyne measurement of the absolute two photon light shift in an optically pumped laser operating at 889 μm, *Opt. Commun.,* **50** (6): 393, 1984.
50. J. Heppner et al., Gain in CW laser pumped FIR laser gases, *IEEE J. Quantum Electron.,* **QE-16** (4): 392, 1980; see also Ref. 49.
51. G. Busse, E. Basel, and A. Pfaller, Application of the opto-acoustic effect to the operation of optically pumped far-infrared gas lasers, *Appl. Phys.,* **17**: 387, 1977.
52. P. M. Plainchamp, Frequency instability measurements of the CH_3OH optically pumped laser at 70.5 and 118 μm, *IEEE J. Quantum Electron.,* **QE-15** (9): 860, 1979.

Eric R. Mueller
DeMaria ElectroOptics Systems, Inc.

SUBPROBLEMS. See Recursion.